

Modeling Sediment Yield with Current and Projected Climatic Scenarios in Andit Tid Watershed, Central Highland of Ethiopia

AYELE DESALEGN WOLDEMARIAM^{1,2}, SAUL DANIEL DDUMBA³, HAILU KENDIE ADDIS⁴

¹ Soil and Water Management Research Directorate, Debre Brihan Agricultural Research Center, Debre Brihan, Ethiopia

² Department of Environmental Management, Makerere University, Kampala, Uganda

³ Department of Geography, Geo-Informatics and Climatic Sciences, Makerere University, Kampala, Uganda

⁴ Soil and Water Management Research Directorate, Amhara Regional Agricultural Research Institute, Bahir Dar, Ethiopia

*Correspondence details: ayeledesalegn5@gmail.com

Submitted on: 2024, 25 April; accepted on 2024, 15 July. Section: Research Papers

Abstract: Our ability to engage in long-term land management solutions that will benefit both land and water users is made possible by our understanding of how climate change affects sediment yield. This study aimed to determine the spatiotemporal distribution of sediment yield in the Andit Tid watershed as well as simulate sediment yield under existing and anticipated climate scenarios. SWAT and Arc GIS 10.5 software were used to estimate and map the spatial distribution of sediment yield. The annual average estimated sediment yield of the watershed was found to be 17.9 t ha⁻¹ yr⁻¹. The R² was found to be 0.62 and 0.72 during calibration and validation of sediment yield. The projected average sediment yield up to 2098 under the wettest scenario is 13.7 t ha⁻¹ in RCP 4.5 and 16.1 t ha⁻¹ in RCP 8.5, respectively. It was discovered that, in comparison to the current average sediment, the near future (2022–2060) sediment was equal to it in RCP 4.5 and decreased by 41% in RCP 8.5, whereas the far future (2061–2098) sediment grew by 20.4% in RCP 8.5 and decreased by 35% in RCP 4.5. Out of the projected 76 years, 21 and 23 years showed positive deviations from the mean of the existing sediment yield under RCP 4.5 and 8.5, respectively. While in the driest scenario, the projected sediment yield was lower than the current rate, which was about 4 t ha⁻¹ in both RCPs. In both current and future climate scenarios, the northeastern, eastern, and western regions were contributing to the higher sediment yield in the watershed. Most of these watershed hotspot regions were situated on farmed land with a slope of more than twenty percent and active gullies. When developing and executing management solutions in the areas that are severely impacted, the watershed community and decision-makers are recommended to make use of the spatial distribution map. It is also necessary to take steps to lessen the likelihood that the emission scenarios that result in RCP 8.5 will occur.

Keywords: Climate, Geospatial, SWAT, SWAT-CUP, Arc GIS

Introduction

Soil erosion is a major issue in most agroecosystems around the world since it is one of the main causes of soil deterioration due to detachment and loss of the topsoil layer (Ahsan et al., 2021). Soil degradation affects 1.9 billion hectares and is growing at a pace of 5-7 million hectares per year globally (IAEA, 2014). Water-induced erosion has been estimated to have harmed 11 million km² of land (Mengie and Teshome, 2019). In Africa, climate change and intensive agricultural practices are among the issues that cause soil erosion (Temesgen and Amare, 2014).

Soil erosion causes decreased soil fertility in Sub-Saharan Africa, resulting in negative environmental consequences (Mengie and Teshome, 2019). Rainfall runoff-induced soil erosion is a major issue in Ethiopia and it is widely regarded as the primary cause of land degradation in the country's rain-fed agricultural areas (Belayneh et al., 2020). The problem of soil erosion has had a significant influence on the productive highlands, which are characterized by rough topography, densely populated, intensive agriculture and a large number of people and cattle (Abebe, 2018; Molla and Sisheber, 2017). Every year, erosion causes the highlands of Ethiopia to lose around 1.5 billion tons of topsoil (Tsegaye, 2019). According to a survey on the economic costs of soil erosion, Ethiopia loses USD 1 billion per year (Tsegaye, 2019). It resulted in the reduction of about 1.5 million tons of crop yield from the country's annual harvest (Taddese, 2001). The Highlands region of Ethiopia accounts for 43% of the total land or 537,000 square kilometers (Hurni, 1988). Those Highlands regions encompass 95% of cultivated land (Shiferaw and Holden, 1999) and account for 90% of the Ethiopian economy. As a result, it is home to 90% of the population and 75% of livestock (Hawando, 1997). The Blue Nile basin, as part of Ethiopia's highlands, loses 131 million tons of soil per year (Tilahun, 2021). Intensive agricultural and other commercial activity has been accelerating soil erosion in the country if no significant policy implications are implemented to protect the land (Adugna, 2015). Estimates produced in the mid-1980s showed that out of a total area of 112 million hectares, 27 million hectares are significantly eroded, 14 million hectares are seriously degraded, and 2 million hectares have reached the irreversible stage (Amsalu and Graaff, 2006). Within the Upper Blue Nile Basin, which covers a total area of 176×10^3 km², 24.4% is experiencing high to severe soil erosion, 12.6% is moderately affected, and 63% is slightly affected by soil erosion (Mengistu et al., 2012).

To balance these ecological processes; human beings' care for soil and water resources is very important. Proper utilization, assessment, and management of the quantity of sediment load and water resources on spatial and temporal scales are mandatory. High sediment rates lead to the filling of reservoirs and loss of live storage, which eventually leads to loss of production potential (Kondolf et al., 2014). The design of effective conservation strategies may need a site-specific assessment of the most influential watershed processes (Addis et al., 2016).

In addressing issues of soil erosion and sedimentation, it is critical to identify affected areas and invest in spatial tools and modeling to manage resources efficiently and effectively. Site-specific assessments of the most influential watershed processes are crucial for the development of efficient conservation measures (Wang et al., 2016). In addition, a better understanding of the factors that determine sediment yield can facilitate and simplify appropriate mitigation.

The soil erosion rate varies due to changes in climatic parameters for a variety of reasons; the most important is the change in the erosive power of rainfall (Tsitsagia et al., 2018).

According to the National Meteorological Agency (2007), climate change is likely to make soil erosion and sedimentation worse. The spatial and temporal variability of rainfall is the factor that leads to the increase and decrease of sediment yield (Tsitsagia et al., 2018). Sediment loading from stormwater runoff can be increased by more frequent and heavy rain events. Stronger storms, higher river levels, and faster stream velocity can exacerbate erosion and increase suspended sediment (turbidity) in water bodies, as well as disrupt the typical sediment distribution along the river, lake, and stream bottoms. The higher temperature might also lead to a higher evaporation rate, while the highest rainfall tends to a higher soil moisture rate that could finally lead to higher erosion (Nearing and Pruski, 2004). The Upper Blue Nile Basin and its major tributaries are subjected to significant environmental degradation (Ayele et al., 2016; Balabathina et al., 2020; Belay and Mengistu, 2021; Betrie et al., 2011; Daniel et al., 2014; Mengistu and Bewket, 2015; Leta et al., 2021; Meresa and Gatachew, 2019).

Ethiopia is one of the countries that is most impacted by rising soil erosion, with a projected 23% increase in soil loss in 2050 (Moges et al., 2020). Thus, quantifying the impact of climate change on sediment yield helps to understand interconnected processes and justifies investment in long-term land management solutions that benefit land and water users (Wallace et al., 2017). Although a large number of research have been conducted to quantify soil erosion in Ethiopia in the current climate, there are very few studies that have projected soil erosion risk in light of the anticipated climate change (Orke and Li, 2022). Furthermore, even though there was no significant trend in the past, as reported by Woldemarim et al, (2023), there is little information currently available regarding the effects of future climate change on sediment in the Upper Blue Nile basins, particularly in the Andit Tid watershed. Modeling is important to project runoff and soil erosion under a dynamic nature to efficiently carry out this type of inquiry (Ahsan et al., 2021). Accurate sediment loss modeling is important for watershed management (Admas et al., 2022; Bayabil and Dile, 2020). Predictive models are useful tools for guiding and informing soil conservation planning and practice. The aim of this study, therefore, was to estimate the watershed average annual net sediment yield, to look at the sediment spatial distribution, and to assess the effects of future climate conditions on sediment yield in the Andit Tid watershed.

Materials and methods

Description of the study area

Andit Tid watershed is one of the seven research stations implemented by the Soil Conservation Research Project (SCRIP). The watershed is approximately 477.6 hectares in size. It is 180 kilometers northeast of Ethiopia's capital, Addis Ababa, at 39°43' east and 9°48' north. The watershed drains westward into the Blue Nile basin, and the river Hulet Wenz drains eastward into the catchment (meaning two rivers in Amharic). The watershed is located on the eastern escarpment of the Rift Valley, which separates the Shewa Plateau from the Awash Plains. The topography varies from 3020 meters above sea level near the outlet in the northwest reach to 3500 meters above sea level in the southeast as illustrated in (Figure 1). Andit Tid Research station is on the eastern edge of the Ethiopian highlands and was chosen as a typical example of highly degraded agricultural zones above 3000 m on the central highlands.

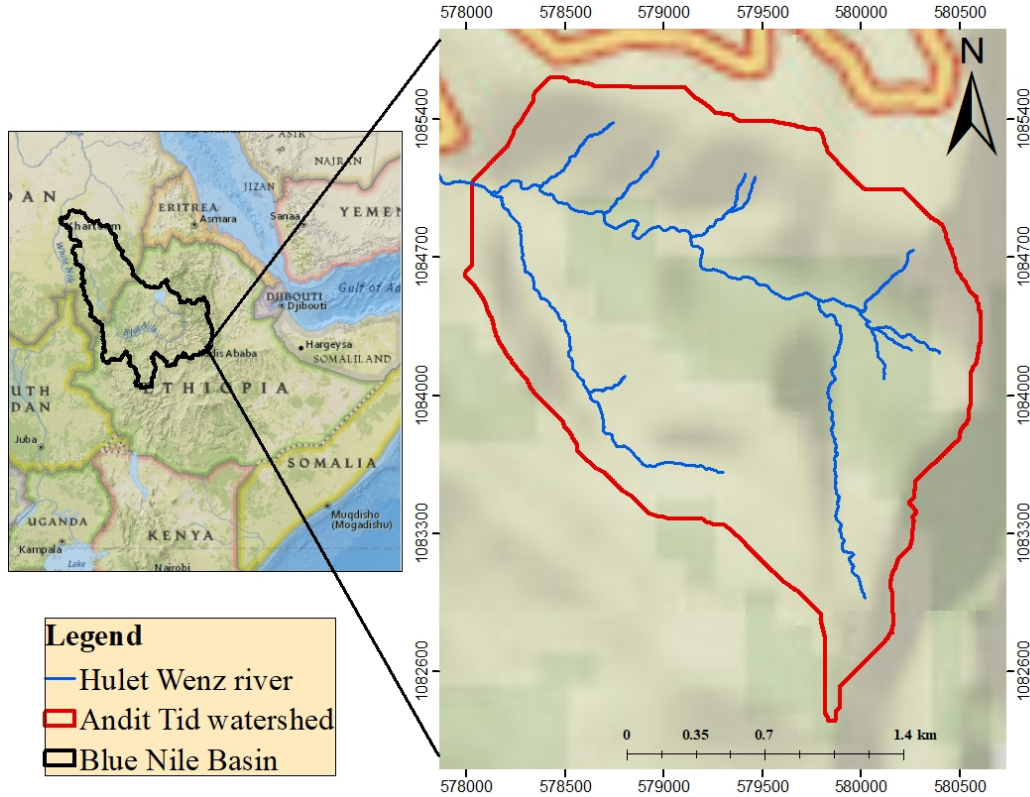


Figure 1 - The location map of the study watershed with the river lines inside.

Gudibado and Wadyat rivers flow from the Northward to the Westward of the watershed, respectively. Their confluence is approximately 150 meters above the gauge station. While the Wadyat River is perennial, Gudibado flows only during the rainy seasons. The watershed is primarily comprised of agricultural land, with the remainder being composed of forest, shrub, grass, and pasture land.

Data sources and method of data collection

Sources of soil map data

This research clipped the raster file to the study watershed from a digital soil map developed by the Food and Agricultural Organization of the United Nations (FAO-UN). Therefore, the clipped soil map of the study watershed was used as an input for the model. The soil map with the resolution of 1km has been derived from Harmonized World Soil Database v1.2 a database that combines existing regional and national soil information and information provided by the FAO soil map (<https://www.fao.org/soils-portal/data-hub/soil-maps-and-databases/harmonized-world-soil-database-v12/en/>). This information included soil texture, hydraulic conductivity, available soil water content, bulk density, soil depth and soil drainage attributes.

Sources of Digital Elevation Model (DEM)

The Digital Elevation Model (DEM) with 2m×2m resolution of the watershed was obtained from the Water and Land Resource Center (WLRC) office in Addis Ababa, Ethiopia. It was used to extract the stream networks, flow direction, flow accumulations, and generations. It also helped to define the watershed and its sub-catchments and to calculate topographic factors such as terrain slope.

Sources of Land Use and Land Cover (LULC) map

The land use of an area is one of the most important factors that affect surface erosion, runoff, and evapotranspiration in a watershed. For this study, the land use land cover map was digitized and classified using Google Earth imagery and Arc GIS 10.5. Supervised classification was done for the identification of land use and land cover types of the study watershed.

Sources of daily climate data (1995 to 2021)

The climate station at the outlet of the watershed, which was managed by the Debre Brihan Agriculture Research Centre and WLRC was used to get the precipitation and minimum (t_{\min}) and maximum temperature (T_{\max}) data needed to run the Soil and Water Assessment Tool (SWAT) model. Four rain gauge sites distributed in the watershed and 3 additional climatic stations (Mezezo, Debre Sina, and Gudoberet) outside of the watershed have been used for modeling. The data for the stations outside the watershed have been obtained from the Ethiopian National Meteorological Agency (ENMA). Since 1995 to 2021, input climatic data have been available in several data formats.

Sources of Projected Climate Data

Coordinated Regional Climate Downscaling Experiment (CORDEX) is experimentally downscaled specifically for climate impact studies in Ethiopia from Africa (Liersch et al., 2018; Liersch et al., 2016). It was designed using multiple Regional Climate Models (RCMs) to provide rationalized, predictable variations in local climates and to evaluate any basis for uncertainty in the projection. RCMs are being used to examine climate projections at the local level (Laprise et al., 2013; Luhunga et al., 2016). According to a previous study by Dosio (2015), RCMs can simulate the most accurate estimates of yearly and seasonal rainfall and air temperature. They are particularly preferred for analyzing the distribution and frequency of extreme rainfall. It also provides climate datasets with a higher spatial resolution and is suited for impact research. The performance of CORDEX in simulating climate variables (rainfall and temperature) is good (Kefeni et al., 2020; Mutayoba and Kashaigili, 2017).

Two representative concentration pathways (RCP) scenarios; the high emission scenario (RCP8.5) and mid-range mitigation emission (RCP4.5) are becoming the most widely used for hydrologic modeling (Vuuren et al., 2011). RCP4.5 suggests that economic structures are rapidly altering to reduce the material intensity and introduce clean energy, with a focus on a universal solution to economic, social, and environmental stability. By the year 2100, the radiative force could have stabilized at 4.5 W/m², never exceeding it. On the other hand, RCP8.5 (Riahi et al., 2007), is a

worst-case scenario (the current trend) with rapid population growth, a slower pace of technological advancement, minimal effort to reduce emissions, and a large reliance on coal-fired power (Vuuren et al., 2011). Due to the strong reliance on fossil fuels, RCP8.5 radiative forcing could peak at 8.5 W/m² by 2100. A detailed description of RCP can be found in (Vuuren et al., 2011). The projected precipitation and temperature data from 11 CORDEX (Table 1) between 2022 and 2098 under RCP 4.5 and RCP 8.5 were downloaded.

Table 1 - List of climate models; their GCM name, RCM name and realization.

Modeling Centre	GCM name	RCM	Ensemble
Canadian Centre for Climate Modeling and Analysis, Canada	CCCma-CanESM2	CRCM4	r1i1p1
Canadian Centre for Climate Modeling and Analysis, Canada	CCCma-CanESM2	RCA4	r1i1p1
The Atmosphere and Ocean Research Institute (The University of Tokyo), National Institute for Environmental Studies, and Japan Agency for Marine-Earth Science and Technology, Japan	MIROC-MIROC5	RCA4	r1i1p1
Bjerknes Centre for Climate Research, Norwegian Meteorological Institute, Norway	NCC-NorESM1-M	RCA4	r1i1p1
Max Planck Institute for Meteorology, Germany	M-MPI-ESM-LR	RCA4	r1i1p1
Max Planck Institute for Meteorology, Germany	MPI-M-MPI-ESM-LR	CFCM5	r1i1p1
Centre National de Recherches Météorologiques, Centre Européen de Recherche et de Formation Avancée en Calcul Scientifique France	CNRM-CERFACS-CNRM-CM5	RCA4	r1i1p1
Geophysical Fluid Dynamics Laboratory, USA	NOAA-GFDL-GFDL-ESM2M	RCA4	r1i1p1
Irish Centre for High-End Computing Ireland European Centre Earth global climate model system	ICHEC-EC-EARTH	HIRHAM5	r3i1p1
Irish Centre for High-End Computing Ireland European Centre Earth global climate model system	ICHEC-EC-EARTH	RACMO22T	r1i1p1
Irish Centre for High-End Computing Ireland European Centre Earth global climate model system	ICHEC-EC-EARTH	RCA4	r1i1p1

Sources of observed sediment data

The staff gauge, automatic runoff stage recorder, and limnigraph are installed at the watershed outlet. Manual river stage recording is done every morning at 08:00. At whatever point there is peak runoff, one-liter grab samples for sediment measurement are taken every 10 minutes starting before as long as the water turns brown. When the water level decreased and the runoff water returned to its original color, the sampling rate decreased to 30-minute interims and after that hour interims. Aside from sediment samples, the river water level is

manually measured to determine total runoff and the suspended material carried by the flow at that particular time interval. By oven-drying the one-liter grab samples and weighing the oven-dried soil, the quantity of sediment load within the sample could be estimated. The total soil loss is then calculated for that sampling interval by multiplying the total water flow per time by the sediment content measured from the one-liter sample. Seven years (2012-2018) of monthly sediment data from the gauge station in the Andit Tid watershed were used to calibrate and validate the SWAT model, including a two-year warmup period.

Conceptual framework

The workflow during the whole life of the research is presented in (Figure 2).

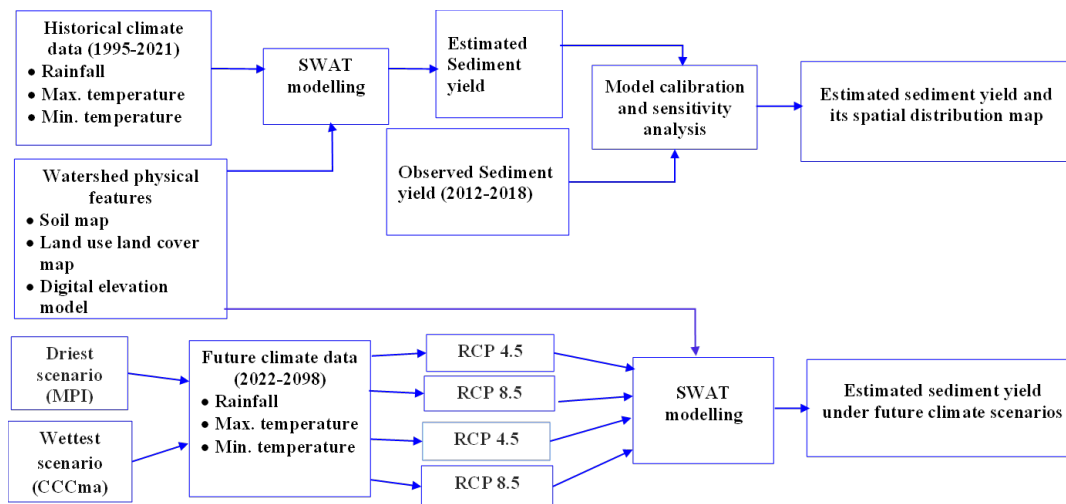


Figure 2 - The procedural skeleton of the whole process of the study

Methods of missing data filling

Missing daily weather data was reproduced using the SWAT weather generator (Schuol, 2007). Outliers from all types of data have been detected using statistical and graphical methods.

Method of simulation of sediment yield

Simulations of sediment yield were done using the SWAT. SWAT is one of the most widely used watershed modeling tools in the world, with applications in a wide range of water quantity and quality issues (Shrestha et al., 2016). SWAT takes into account factors such as weather, surface runoff, evapotranspiration, irrigation, sediment transportation, groundwater flow, crop growth, nutrient yielding, pesticide yielding, and water routing, as well as the long-term consequences of various agricultural management strategies (Arnold et al., 2011; NEITSCH et al., 2005).

In the hydrological component, the total runoff for the watershed is calculated by routing the predicted runoff separately for each sub-basin of the total watershed area. Using a modified version of the universal soil loss equation (MUSLE), the sediment yield is calculated (eqs 6). The watershed is divided into sub-basins in the SWAT model, and these sub-basins are further divided into one or more homogeneous hydrological response units

(HRUs) with relatively unique combinations of land cover, soil and topographic conditions. The model could produce summary statistics per sub-basins or HRUs as an output. Therefore, it was possible to identify sediment hotspot regions or sub-basins using the output map. The water balance equation was used to estimate the total soil water content in the watershed (eqs 1).

$$SW_t = SW_0 + \sum_{i=1}^n (R - Q - ET - W_{seep} - Q_{gw}) \dots\dots\dots(1)$$

Where SW_t is the final soil water content (mm), SW_0 is the initial soil water content (mm), t is time in days, R is precipitation (mm), Q is surface runoff (mm), ET is the evapotranspiration (mm), W_{seep} is percolation (mm), and Q_{gw} is return flow (mm).

In this study, the Hargreaves method (eqs 2) was used to determine potential evapotranspiration because rainfall and minimum and maximum temperatures were the only climate data available as recommended by (Hargreaves, 1985; Yates and Strzepe, 1994).

$$ET_0 = 0.0023 * 0.408 * R_a(T_{mean} + 17.8)(T_{max} - T_{daily})^{0.5} \dots\dots\dots(2)$$

T_{mean} is the maximum air temperature (C), T_{daily} is the average air temperature (C), R_a is extraterrestrial radiation (MJm^{-2}), and 0.408 is a factor to convert $MJ m^{-2}$ to mm. R_a is an estimate of extraterrestrial radiation based on the location's latitude and the calendar day of the year.

SWAT employs two approaches based on the aforementioned assumption to estimate surface runoff; the Green and Ampt infiltration method and the Soil Conservation Service curve number (SCS) method (Zhang et al., 2019). SCS is widely utilized due to its ability to employ daily input data. This study used the Soil Conservation Service curve number (SCS) method to assess surface flow. Mathematically, surface runoff has been estimated as (eqs 3):

$$Q_{surf} = \frac{(R_{day}-0.2)^2}{(R_{day}+0.8S)^2} \dots\dots\dots(3)$$

where: Q_{surf} is the accumulated runoff or rainfall (mm), R_{day} is the rainfall depth for the day (mm), and S is the retention parameter (mm) (eqs 4):

$$S = 25.4 * \left(\frac{100}{CN} - 10\right) \dots\dots\dots(4)$$

SWAT uses a modified rational method to compute the peak runoff rate. The rational technique assumes that the intensity of precipitation begins at a time $t=0$ and continues indefinitely, with the rate of runoff increasing until $t=t_{conc}$, the time of concentration. The modified rational technique is stated mathematically as follows (eqs 5):

$$q_{peak} = \frac{(at_c * Q_{surf} * A)}{(3.6 * t_{conc})} \dots\dots\dots(5)$$

where, q_{peak} is the peak runoff rate (m^3/s), at_c is the fraction of daily precipitation that occurs during the time of concentration, Q_{surf} is the surface runoff (mm), A is

the sub-basin area (km^2), t_{conc} is the time of concentration (hr), and 3.6 is the conversion factor.

Finally, the SWAT model calculates surface sediment caused by rainfall and runoff within each HRU using the modified universal soil loss equation (Williams, 1975).

$$\text{Sed} = 11.8 (\text{Qsurf} * \text{qpeak})^{0.56} * K * LS * C * P \dots\dots\dots(6)$$

Where: Sed represents the sediment yield per event (metric tons), K denotes the soil erodibility factor, LS denotes the topographic factor, C is the cover management factor, and P is the support practice factor.

Data preparation for the SWAT model

Climate data preparation

The SWAT model was developed using meteorological data including rainfall data from seven stations and temperature data from four stations. The SWAT format was used to compile the available climatic data and their matching location table, which was then incorporated into the model using the weather data input wizard. *swat-weatherdatabase-v01803*, a user-friendly program for archiving and processing daily weather data to be used with SWAT projects (Essenfelder, 2016).

Soil data preparation

The user soils were imported and added to the SWAT soil database to incorporate the soil parameters in the SWAT-2012 geodatabase. The dominant soils in the watershed were eutric Leptosols and lithic Leptosols, which cover 55.7 % and 37.6 %, respectively. Eutric Cambisols is another third soil type found in the easternmost part of the watershed, covering only 6.7 % of the watershed area. All the data were obtained from FAO soil databases and the water balance model for the eastern Nile basin (Hassan, 2012).

Digital elevation model (DEM) preparation

The DEM has been used to describe the topography and the geometry of the watershed (Figure 3). The spatial distribution of erosion is highly dependent on the topographic characteristics of an area. A steeper slope causes higher runoff velocities, more splashes downhill, and faster flow, and therefore contributes to greater soil erosion. The steep and rugged terrains are a defining feature of the Andit Tid watershed. More than half of the watershed has a slope of 20 % or steeper. The slope steepness increased significantly following the sides of the two rivers; Wadiat and Wani-Gedel.

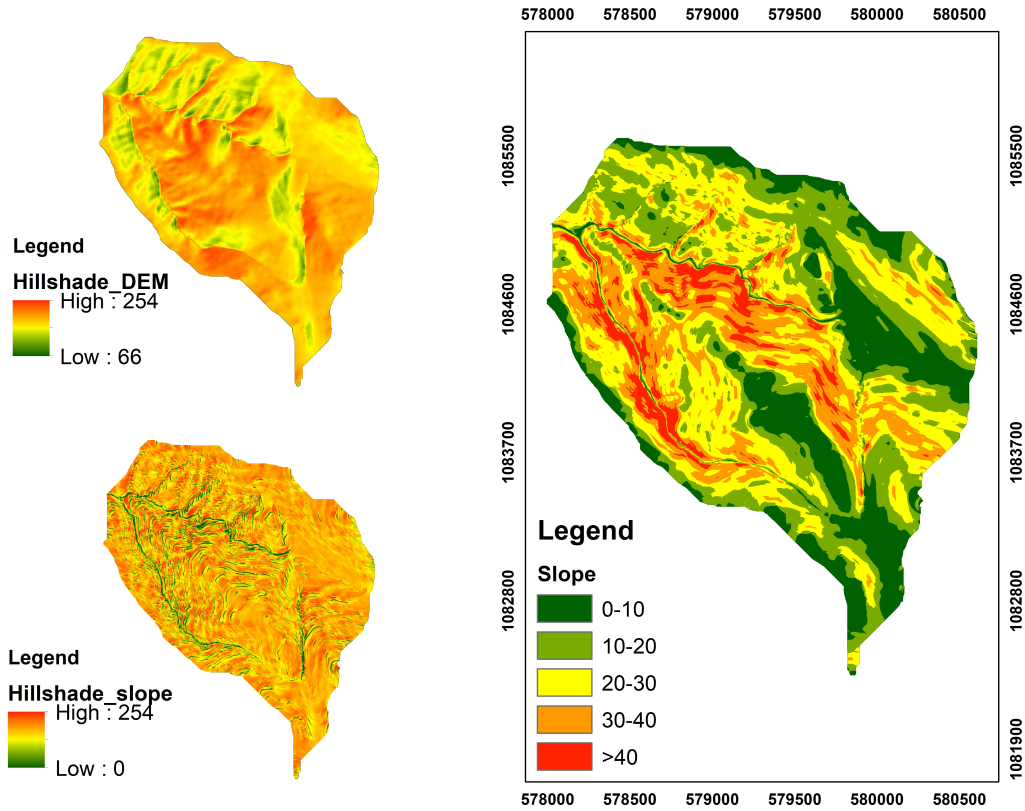


Figure 3 - A hill shade DEM, hill shade slope, and slope class map of the study watershed: the steepest areas are colored in red, while the flattest parts are shaded in green.

Land use and land cover (LULC) map preparation

The analysis of land use and land cover (LULC) of the watershed was conducted using cloud-free Landsat 9 imagery. The image processing involved band composition and supervised classification techniques to categorize different types of land use. A maximum likelihood supervised classification was performed using ArcGIS 10.5, identifying six major LULC types within the watershed: agricultural land, forest land, open forest land, grassland, bushland, and open grasslands.

The classification results indicated that agricultural land is the predominant land use type, covering approximately 60% of the total watershed area. This is followed by bushland, which accounts for 14.71% of the area. Open forest land is the least common land use type, constituting only 0.7% of the total watershed area. The detailed area coverage for each land use type is presented in Table 2.

Table 2 - The land use and land cover types and their respective proportional coverage of the watershed

Landuse	SWAT-code	Area [ha]	Percentage
Agricultural Land	AGRL	286.07	60
Dense forest land	FRSE	43.59	9.1
Open forest	FRST	3.48	0.7
Bush land	RNGE	70.23	14.7
Grassland	SPAS	22.66	4.74
Open grassland	PAST	51.59	10.8
Total		477.6	100.0

As a deterministic tool, SWAT has its method for preparing the input data. All land use types in the SWAT database are coded with four letters as part of the input parameter used in SWAT modeling. Each land use recognized in the study watershed has a four-letter code (Table 2), based on the SWAT database.

Watershed and sub-basin delineation

The model automatically delineated a watershed of 477.6 ha and 27 sub-basins. From the total of 27 sub-basins, sub-basins 22, 5, and 7 were the smallest, while sub-basins 24, 19, and 20 were the largest sub-basins with the minimum flow accumulation threshold area of 2.5 ha (6250 grids, 4 m² each).

Hydrological Response Unit (HRU) definition

The delineated watershed by Arc SWAT and the prepared land use overlapped 100%. The 6 classes land use map was reclassified into 6 classes to correspond with the land use in the SWAT interface based on the study (Setegn et al., 2008). The HRU analysis in Arc SWAT includes divisions of HRUs by slope classes in addition to land use and soil. The slope discretization (0-10, 10-20, 20-30, 30-40, >40) which accounts for the lower slope ranges is the best discretization option in considering the deposition of soil materials during sediment transportation (Setegn et al., 2008 and Ashagre, 2009).

Model Sensitivity, Calibration, and Validation

The Sequential Uncertainty Fitting (SUFI-2) algorithm associated with SWAT-CUP 2012 has been used for a combined model sensitivity analysis, calibration, and validation procedures. The SUFI-2 algorithm considers both uncertainties of the conceptual model and uncertainties of the input data (Gupta and Beven, 2006).

After the model was set up, the next step was to run the model. The results from the simulation cannot be directly used for further analysis but instead, the ability of the model to sufficiently predict the constituent sediment yield should be evaluated through sensitivity analysis, model calibration, and model validation (White and Chaubey, 2005). The sensitivity analysis aims to estimate the rate of change in the output of a model concerning changes in watersheds that result in a clear difference in hydrologic sensitivity (Reungsang et al., 2007). To better understand the behavior of the hydrological system, evaluate the

applicability of the model, and identify the parameters required to improve the simulation results, sensitivity analyses were carried out. Parameters for sensitivity analysis were selected by reviewing previously used calibration parameters and documentation from the SWAT manuals and other scholars (Feyereisen et al., 2007; Roth et al., 2016; NEITSCH et al., 2005; Saha et al., 2014; Smith et al., 2008; Yimer, 2015; White and Chaubey, 2005; Zhang et al., 2007)

Model calibration is the modification of parameter values and comparison of the predicted output of interest to measured data until a defined objective function is achieved (Das et al., 2019; Khanal and Parajuli, 2014). Additional parameters, other than those identified during sensitivity analysis, are used primarily for calibration due to the hydrological processes naturally occurring in the watershed. Sediment yield calibration was done using and adjusting parameters that affect the sedimentation processes. Validation for sediment yield was done immediately after the model was successfully calibrated. Monthly average data from 2012-2015 and 2016-2018 of sediment yield have been used for calibration and validation, respectively.

The 95 percent probability distributions produced at 2.5 percent and 97.5 percent of the cumulative distribution resulting from the propagation of parameter uncertainty, which is referred to as the 95 percent prediction uncertainty (95PPU), was used to express the uncertainty of the output variables (Abbaspour, 2015; Dakhlalla and Parajuli, 2019).

The goodness of fit of the model

Coefficient of determination (R^2) (Krause et al., 2005), Nash-Sutcliffe efficiency (NSE) (Nash, 1970) percent bias (PBIAS) (Gupta and Sorooshian, 1999), Kling and Gupta Efficiency (KGE) (Gupta et al, 2009) and p-factor have been considered during the evaluation of the goodness of fit of the model.

The NSE is a normalized statistic that assesses the relative magnitude of residual variance when compared to observed data (eqs 7) (Nash, 1970). It also showed how well the plot of observed versus simulated data follows the 1:1 line. NSE is the most common; emphasizes high flow; neglects the low flows and is a distance-based evaluation method (Krause et al., 2005; McCuen et al., 2006). The model performance can be determined by the value of NSE, which can be $0.75 < NSE \leq 1$, $0.65 < NSE \leq 0.75$, $0.5 < NSE \leq 0.65$, $0.4 < NSE \leq 0.5$ and $NSE \leq 0.4$, with very good, good, satisfactory, acceptable, and unsatisfactory, respectively (Boskidis et al., 2012; Moriasi et al., 2007).

$$NSE = 1 - \frac{\sum(Q_m - Q_s)^2}{\sum(Q_m - \bar{Q}_m)^2} \dots \dots \dots (7)$$

Nash and Sutcliffe (1970), Q and \bar{Q} are individual observation and mean values of the variable (sediment), respectively, m and s are measured and simulated values of the variable.

The R^2 measures the proportion of variance in observed data and spans from 0 to 1, with higher values implying less error variance. The R^2 value could indicate the model's performance as very good, good, satisfactory, and unsatisfactory with values of, $0.7 < R^2 \leq 1$, $0.6 < R^2 \leq 0.7$, $0.5 < R^2 \leq 0.6$, and $R^2 < 0.5$, (eqs 8) respectively (Moriasi et al., 2007).

$$R^2 = \frac{\sum[(Q_m - \bar{q}_m)(Q_s - \bar{q}_s)]^2}{\sum(Q_{mi} - \bar{q}_m)^2 \sum(Q_s - \bar{q}_s)^2} \dots\dots\dots(8)$$

where: Q and \bar{q} are individual observations and mean values of the variable (sediment), m and s are measured and simulated values of the variable.

The average tendency of simulated data to be larger or smaller than their observed counterparts is measured by percent bias (PBIAS). It has an ideal value of 0, and low magnitude values indicate accurate model simulation. Positive values indicate underestimation bias in the model, whereas negative values suggest overestimation bias in the model (Gupta and Sorooshian, 1999). PBIAS is monotony and cannot be used as a decision-making criterion alone, but in collaboration with other criteria statistics, it might determine the model as very good, good, satisfactory, and unsatisfactory with the value $PBIAS < \pm 10$, $\pm 10 < PBIAS < \pm 15$, $\pm 15 < PBIAS < \pm 25$ and $PBIAS > \pm 25$ respectively (Legates et al., 1999). Mathematically PBIAS can be calculated as (eqs 9):

$$PBIAS = \left[\frac{\sum_{i=1}^n (Q_i m - Q_i s) * 100}{\sum_{i=1}^n Q_i m} \right] \dots\dots\dots(9)$$

KGE is reproduced by the Euclidian distance of the three variables derived from the NSE (eqs 10). The values of KGE range from $-\infty$ to 1, and the optimal value is 1 (Gupta et al., 2009).

$$KGE = 1 - \sqrt{(\alpha - 1)^2 + (\beta - 1)^2 + (r - 1)^2} \dots\dots\dots(10)$$

Where; $\alpha = \frac{\sigma_s}{\sigma_o}$ is the relative variability measured by the standard deviation values σ_s and S_i and σ_o of O_i ; $\beta = \frac{\mu_s}{\mu_o}$ is the ratio of the mean between the simulated and observed data and r is the linear correlation coefficient between S_i and O_i .

The p-factor, or percentage of data bracketed by the 95% prediction uncertainty (95PPU), indicates how well the uncertainty ranges cover the observed data. It's a measure used in the SUFI-2 algorithm within SWAT-CUP to evaluate the quality of calibration (Dakhllalla and Parajuli, 2019; Mengistu et al., 2019; Yesuf et al., 2015). A higher p-factor means a higher percentage of observed data points are within the prediction uncertainty range.

Climate Model Performance Evaluation

Taylor diagrams were recently introduced graphical evaluation technique used to visually show which of the climate models is the most accurate. The Pearson correlation coefficient, the root means square error, and the standard deviation are used to measure the degree of agreement between the modeled and observed. Simulated patterns that closely resemble observations have been located closest to the x-axis point labeled “observed”. Taylor's diagram is used as a decision-making criterion for the confusing result of the statistical criteria (Taylor, 2001). This diagram provides a way of plotting three statistics on a 2-D graph that indicates how closely a pattern matches observations (Taylor, 2001). This diagram is a newly introduced 2D tool designed to clarify confusing statistical results in climate model evaluation and is currently used by many scholars (Getaneh Ayele et al., 2024; Izzaddin et al., 2024; Sa’adi et al., 2017; Tegegne and Melesse, 2020; Xiong et al., 2021).

The model MPI (CRCM5), MPI (RCA4), and CNRM-CERFACS-CNRM-CM5 have about the same correlation ($r=0.8$) with the observed maximum temperature (Figure 4). NorESM1-M is the less accurate model; it has a low pattern correlation with the observed maximum temperature.

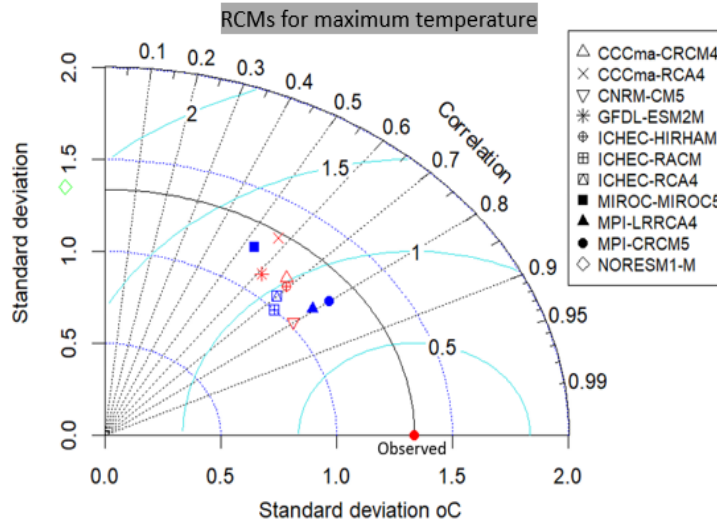


Figure 4 - Pattern statistical comparison between the observed maximum temperature and the eleven climate models.

The observed minimum temperature was strongly correlated ($r>0.9$) with all of the climatic models. CCCma-RCA4 has a relatively lower standard deviation, which is to the x-axis point labeled "observed," as seen in (Figure 5). Yet, this assessment proved that the climate models are appropriate for predicting the study area's future minimum temperature.

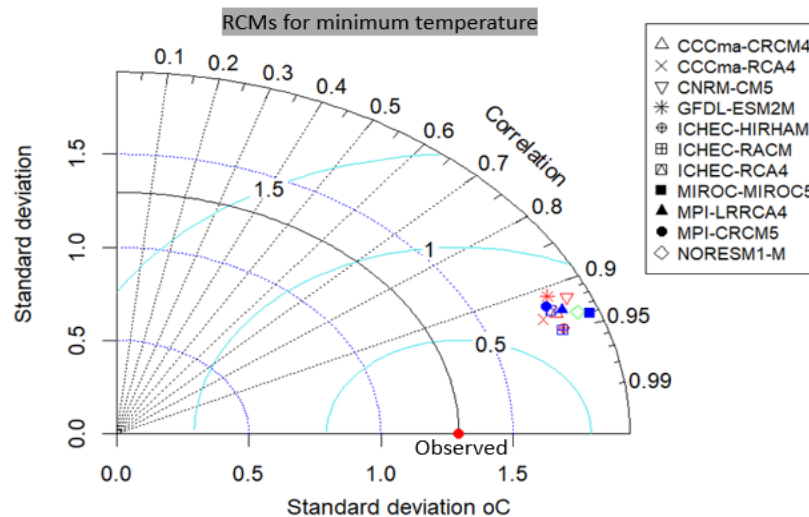


Figure 5 - Pattern statistical comparison between the observed minimum temperature and the eleven climate models.

The ICHEC-HIRHAM and MPI-CRCM5 climate models were shown to be better than the others in terms of rainfall projection. They are more correlated ($r \approx 0.8$) with the actual rainfall. The only model that has the lowest correlation ($r < 0.5$) with the observed and is furthest from the x-axis labeled "observed" is NORESM1-M (Figure 6). The remaining climate models have all correlated satisfactorily with the actual rainfall.

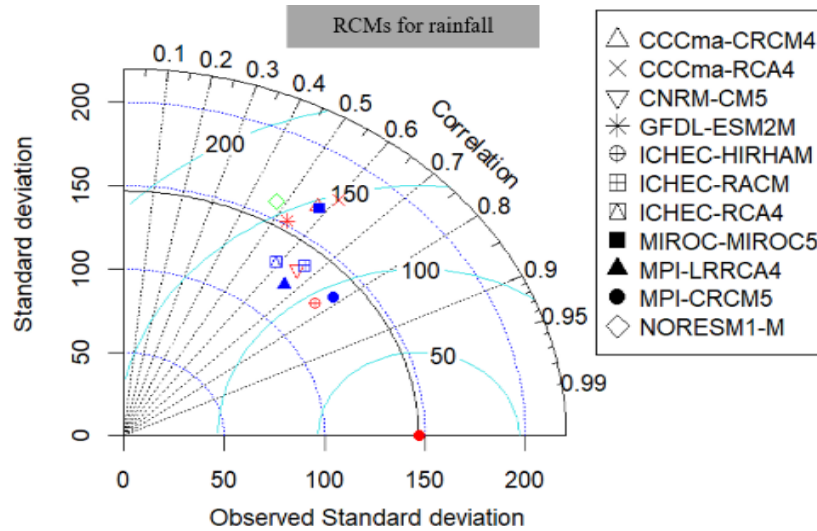


Figure 6 -Pattern statistical comparison between the observed rainfall and the eleven climate models.

From the evaluation, all climate models were found to be suitable to project the future climate condition of the study area other than NorESM1-M. Therefore, this study used two climate models having the highest and the lowest annual rainfall to look at the future sediment yield in both dry and wet scenarios. The regional climate model MPI (RCA4) and CCCma (CRCM4) were found to be the driest and the wettest climate models, respectively. The observed data and these climate models show a strong correlation (Figure 4-6).

Bias correction for climate data

After the selection of the best models for the study area, the climate model data for hydrological modeling (Cmhyd) have been used to do bias correction (Rathjens et al., 2016 and Bieger et al., 2017). Cmhyd is a Python tool designed to integrate global and regional climate model data into hydrological models. It performs temporal and spatial bias correction on climate model data, ensuring it accurately reflects the observation gauges used in hydrological model inputs (Zhang et al., 2018; Rathjens et al., 2016). The future periods of 2022 to 2098 were simulated against the 1991 to 2010 baseline period. Local intensity scaling (LOCI) was used in precipitation bias correction and distribution mapping (DM) (Zhang et al., 2018) was used for the bias correction of the temperature.

Projected rainfall and temperature trend analysis

The Mann-Kendall (MK) trend test was used to detect long-term future trends in rainfall and temperature derived from both the driest and wettest climate models. This time series trend analysis was conducted using the trial version of XLSTAT software. The MK test, a

rank-based method, is particularly suited for trend analysis of time series data, helping to identify whether there is a statistically significant trend over time (Burn et al., 2004 and Tesemma et al., 2010). The normalized test statistics Z for the MK test are computed using Eqs. (11)-(14) below (Yu et al., 1993).

$$S = \sum_{i=1}^{n-1} \sum_{j=i+1}^n \text{sgn}(x_j - x_i) \dots \dots \dots (11)$$

Where;
$$\text{sgn}(x_j - x_i) = \begin{cases} +1 & \text{if } (x_j - x_i) > 0 \\ 0 & \text{if } (x_j - x_i) = 0 \\ -1 & \text{if } (x_j - x_i) < 0 \end{cases} \dots \dots \dots (12)$$

sgn is the signum function and xi and xj are the annual values in the years i and j, i > j, respectively,

The application of the trend test is done to a time series Xi that is ranked from i = 1, 2...n-1 and Xj, which is ranked from j = i + 1, 2.... n. Each of the data points Xi is taken as a reference point which is compared with the rest of the data point's Xj so that:

If S>0, then later observations in the time series tend to be larger than those that appear earlier in the time series and it is an indicator of an increasing trend, while the reverse is true if S<0 and this indicates a decreasing trend.

Under the null hypothesis of no trend, the statistic S follows an approximately normal distribution with mean zero and variance (Kendall, 1975) statistic is given as:

$$\text{var}(S) = \frac{n(n - 1)(2n + 5) - \sum_{t=1}^m t_1(t_1 - 1)(2t_1 + 5)}{18} \dots \dots \dots (13)$$

Where: n is the number of observations and ti are the ties of the sample time series. And m is the number of tied groups.

When the sample size n ≥ 10, as used in this study, the test statistic Z is calculated as (Kendall, 1975).

$$Z = \begin{cases} \frac{S - 1}{\sigma} & \text{if } S > 0 \\ 0 & \text{if } S = 0 \\ \frac{S + 1}{\sigma} & \text{if } S < 0 \end{cases} \dots \dots \dots (14)$$

Where: Z follows a normal distribution, a positive Z and a negative Z depict an upward and downwards trend for the period respectively.

Sediment yield modeling with future climate scenarios

SWAT was run with bias-corrected projected climate data from the two models for the near future and the far future. The impact of climate conditions with both RCP 4.5 and RCP 8.5 on sediment yield was then determined by comparing the current with projected outputs. In all scenarios, the spatial distribution and hot spot area mapping were done using Arc GIS 10.5.

Results

Sensitive parameters during sediment simulation

Sensitivity analysis was done using eleven parameters (Table 3). The analysis indicated SOL_AWC(..).sol, SOL_K(..).sol, SPCON.bsn, and USLE_P were the most sensitive parameters for simulating sediment yield.

Table 3 - Parameter sensitivity, method of a parameter change, initial intervals and fitted values

Parameter Name	Descriptions	Min-value	Max-value	Fitted Value	t-Stat	P-Value
R__SOL_AWC(..).sol	Available water capacity of the soil layer.	-0.25	0.25	0.0441	0.406	0.000
R__SOL_K(..).sol	Saturated hydraulic conductivity.	-0.15	0.25	0.17	0.285	0.000
V__SPCON.bsn	Linear parameter for calculating the maximum amount of sediment that can be reentrained during channel sediment routing.	0.0001	0.01	0.007	-2.361	0.024
V__USLE_P.mgt	USLE equation support practices Plant uptake compensation factor.	0.16	0.91	0.279	0.601	0.327
A__EPCO.hru	USLE soil erodibility	0	1	0.616	0.960	0.344
R__USLE_K(..).sol	Groundwater "revap" coefficient.	0.27	0.78	0.510	-0.649	0.521
A__GW_REVAP.gw	Manning's "n" value for the main channel.	0.02	0.2	0.122	0.548	0.587
V__CH_N2.rte	Groundwater delay (days).	0	0.2	0.072	0.454	0.653
A__GW_DELAY.gw	Soil evaporation compensation factor	0	500	191.8	-0.453	0.654
A__ESCO.hru	Exponent parameter for calculating sediment reentrained in channel sediment routing.	0	1	0.914	0.416	0.680
V__SPEXP.bsn		1.0	1.5	1.189	0.338	0.738

V_ means the existing parameter value is to be replaced by the given value

A_ means that the given value is added to the existing parameter value

R_ means that the value of the existing parameter is multiplied by (1+ a given value)

The model performed well to simulate the sediment yield in the Andit Tid watershed. The P factor was calculated to evaluate the uncertainty of the model. They implied that 71% and 72% of the observed sediment were enveloped by the 95PPU during the calibration (2012-2015) and validation period (2016-2018), respectively as illustrated in Figure 7.

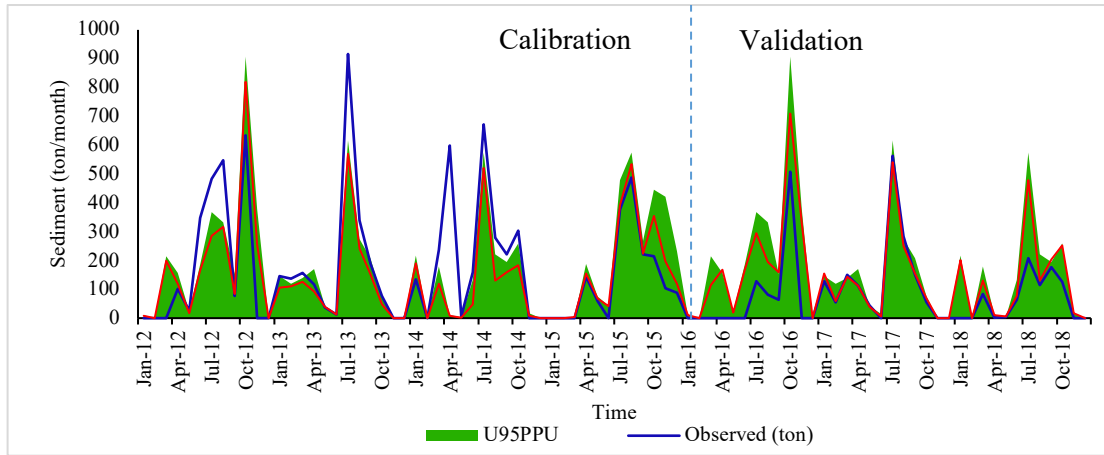


Figure 7 - Comparison of the measured and predicted monthly sediment yield during the calibration (2012-2015) and validation (2016-2018) period.

The R^2 was 0.64 and 0.72 and PBIAS was determined to be 34.5 and 33.5 during calibration and validation, respectively. Additionally, KGE was determined to be 0.4 and 0.34 during calibration and validation, respectively. The model is generally good at simulating the sediment yield of the Andit Tid watershed (Table 4).

Table 4. Summary statistics for calibration and validation of sediment yield in the outlet of the Andit Tid watershed

Variable	Tests	Objective functions				
		R^2	PBIAS	NSE	p-factor	KGE
Sediment yield	Calibration	0.64	34.5	0.5	0.71	0.4
	Validation	0.72	33.8	0.52	0.72	0.34

Simulated and observed sediment yield

The correlation between the predicted and observed sediment yield was found statistically significant with a correlation coefficient of ($r = 0.82$) at ($p < 0.01$) level of significance. As shown in (Figure 8), the one-unit change in observed sediment will have a 0.44-unit change in the predicted sediment yield.

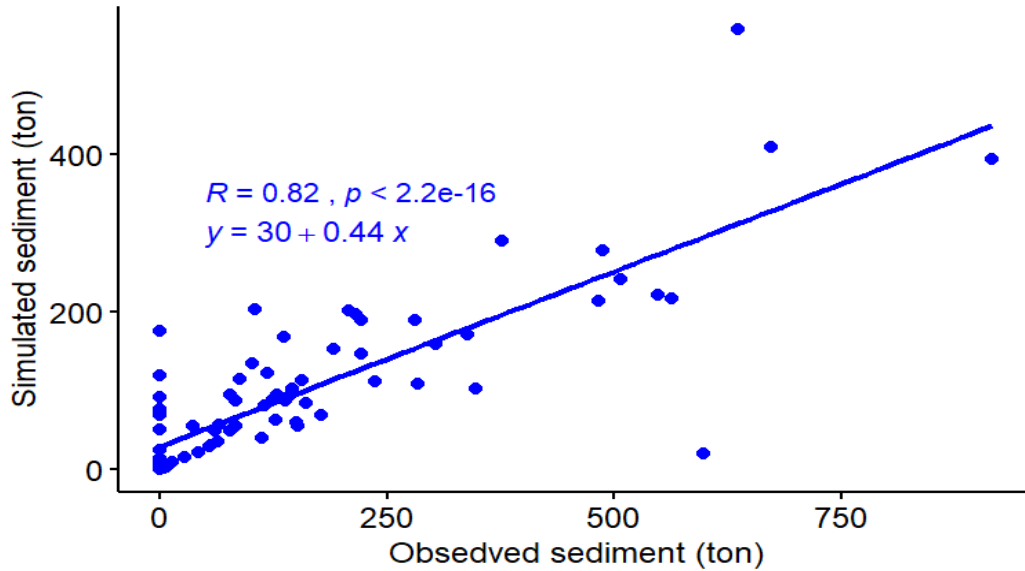


Figure 8 - The 1:1 scatter chart between simulated and observed sediment yield with a correlation value

Estimation and hotspot area mapping of sediment with current climate condition

The total annual sediment loss of the watershed is estimated at 8543.52 tons, with a significant variation in erosion vulnerability across the sub-basins. The study highlights that 17 out of the 27 sub-basins exceed the tolerable soil loss levels for Ethiopia's highlands, which range from 2 to 18 t ha⁻¹ yr⁻¹, according to Hurni (1993). This finding underscores the urgency of targeted soil conservation interventions in these areas.

Sub-basin 8 stands out as the most vulnerable, with an alarming sediment loss rate of 43.5 t ha⁻¹ annually, far exceeding the upper limit of the tolerable range. This high rate of sedimentation suggests severe land degradation, likely due to factors such as steep slopes, deforestation, overgrazing, and inadequate soil conservation practices. On the other hand, sub-basin 25, with an annual sediment loss of only 0.28 t ha⁻¹, is the least affected. This disparity between sub-basins 8 and 25 highlights the heterogeneity within the watershed, pointing to the need for localized soil conservation strategies.

The average annual sediment loss for the watershed is 17.9 t ha⁻¹. This average, however, masks the extreme variations within the watershed, as evidenced by the wide range of sediment loss values. The visual illustration (Figure 9) supports this by color-coding the sub-basins based on their vulnerability, with green indicating the safest areas and red/orange indicating the most vulnerable. The spatial distribution of sediment loss vulnerability indicates that sub-basins in the Northeastern, Eastern, and Western regions are particularly prone to erosion. Specifically, sub-basins 7, 8, 10, 14, and 18 in the northern to eastern section, and sub-basins 18, 23, and 24 in the central and western parts, are identified as high-risk areas. These regions likely experience higher erosion due to a combination of natural and anthropogenic factors, including topography, soil type, land use practices, and climatic conditions. Conversely, sub-basins located in the center of the watershed, such as 15, 13, 20, 9, 11, 12, and 16, along with sub-basin 25 in the southeastern part, exhibit lower sediment

loss rates. These areas may benefit from more effective soil conservation practices, flatter terrain, better vegetation cover, or less intensive land use.

The findings underscore the need for targeted soil and water conservation measures in the most vulnerable sub-basins. Interventions could include reforestation, terracing, the establishment of grass strips, and the adoption of sustainable agricultural practices. Given the high variability in erosion rates, conservation efforts should be tailored to the specific conditions of each sub-basin to be most effective. Continuous monitoring and adaptive management are essential to address the dynamic nature of soil erosion and sediment loss in the watershed.

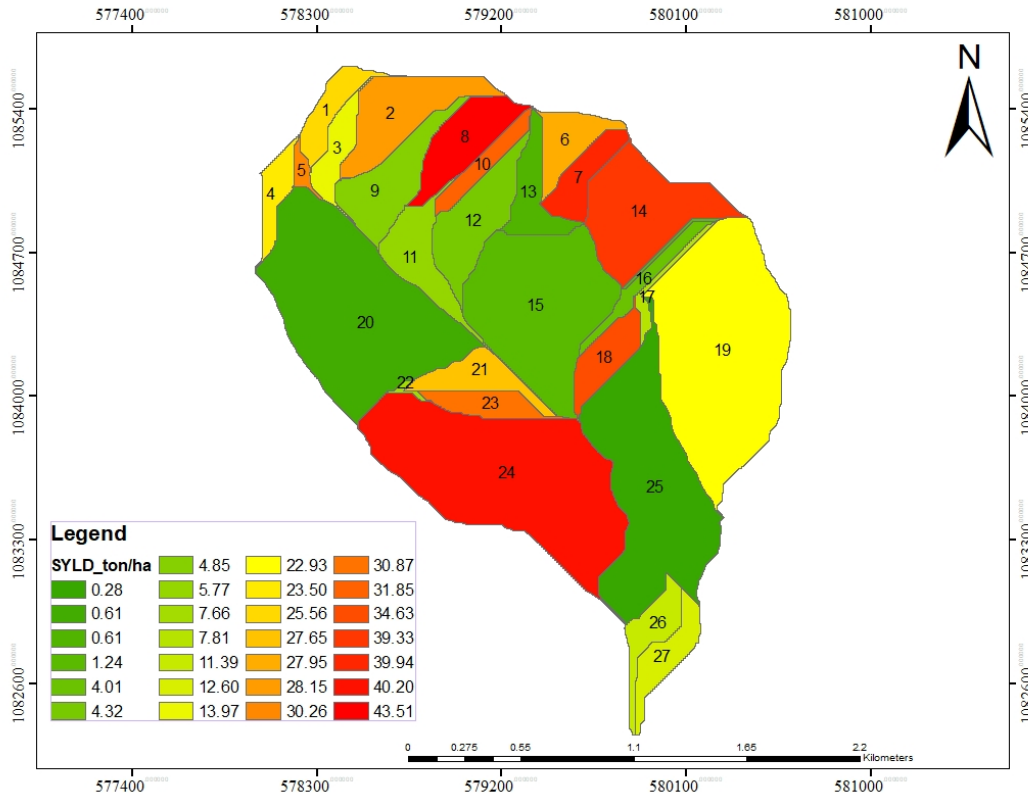


Figure 9 - Estimated sediment yield per sub-basins of Andit Tid watershed (the red and yellow shaded are identified to be highly affected while the green shaded are less affected sub-basins).

Projected temperature and rainfall

In 2098, the average yearly rainfall of the Anit Tid watershed will be 1451.7 mm, with a range from 468.3 mm to 3812.1 mm in RCP 4.5 and 1561.5 mm, with a range from 563.2 mm to 4541.1 mm in RCP 8.5, respectively. The average rainfall in the near future (2022-2060) would be 1572.05 mm and 1352.4 mm in RCP 4.5 and RCP 8.5, respectively. The annual rainfall could then drop by 247.78 mm to 1328.27 mm in RCP 4.5 and rise by 432.63 mm to 1776.03 mm in RCP 8.5 in the far future (2061-2098). Therefore, as RCP 4.5 projects, the annual rainfall in the mid-century will be greater than the annual rainfall in the late century, while as RCP 8.5 projects the rainfall will continuously be increased up to 2098.

In regards to temperature, the study watershed's projected temperature under RCP 4.5 and RCP 8.5 will be 19.3°C and 20.5°C, respectively. The temperature of the study watershed showed an increase over time in both RCPs, as presented in Figure 10. RCP 4.5 and RCP 8.5 project that in the near-future (2022–2060), the average temperature may be 19°C and 19.6°C, respectively. In the long periods of time (2061–1998), it is projected that the temperature will increase by 0.7°C and 1.8°C, respectively, for RCP 4.5 and RCP 8.5.

Trends of projected temperature and rainfall

The trend analysis of the projected temperature and rainfall from both the wettest and driest climate models is illustrated in Figure 10. The figure evidences an increasing trend for all temperature measurements across climatic models and RCPs. Conversely, the graph for rainfall exhibits an undefined trend in both climate models and RCPs. Therefore, it was crucial to perform a Mann-Kendall trend analysis (Table 5) to accurately determine whether there were any significant increasing or decreasing trends in the projected rainfall and temperature for the study watershed.

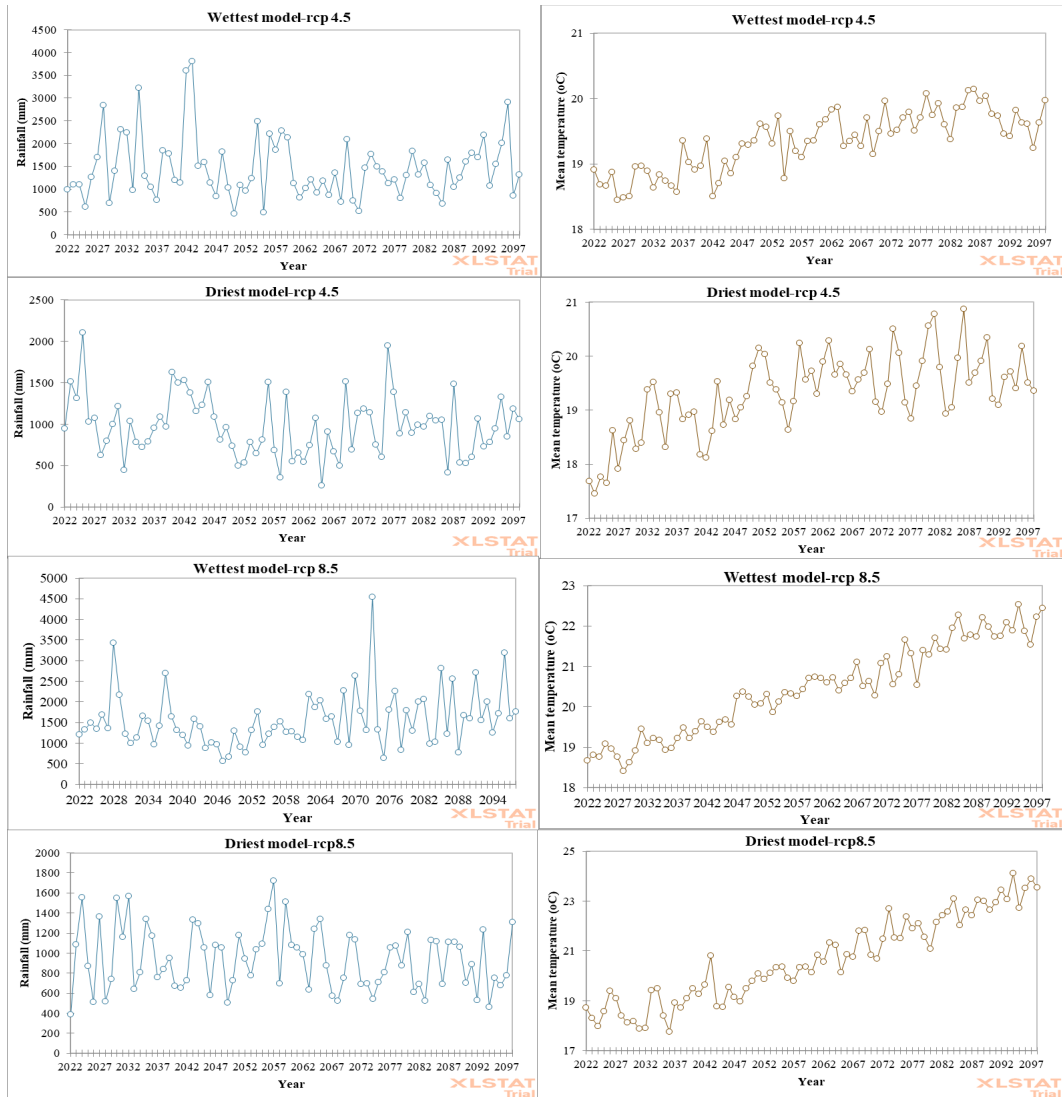


Figure 10 - The chart shows the time series trends of projected rainfall and temperature of the wettest and driest RCMs with RCP 4.5 and RCP 8.5.

The Mann-Kendall trend test results for the projected rainfall and temperature of the driest and wettest climate models are presented in Table 5. From Table 5, it can be confirmed that in both the wettest and driest climate models, the temperature is significantly increasing. In contrast, rainfall is decreasing in the driest climate model across both RCPs, though this decrease is not statistically significant. Rainfall is significantly increasing in the wettest climate model under RCP 8.5, while in the wettest climate model under other RCPs, there is a non-significant increase.

The Sen's slope (S value) is positive for all temperature results, indicating an increasing trend. Conversely, a negative S value for rainfall suggests a decreasing trend. However, the magnitude and significance of these trends vary between the climate models and RCPs.

Table 5 - The Mann-Kendall trend test result for the projected rainfall and temperature with the driest and wettest climate models and RCPs.

	Temperature				Rainfall			
	Driest RCMs		Wettest RCMs		Driest RCMs		Wettest RCMs	
	RCP 8.5	RCP 4.5	RCP 8.5	RCP 4.5	RCP 8.5	RCP 4.5	RCP 8.5	RCP 4.5
Kendall's tau	0.82	0.44	0.85	0.6	-0.08	-0.08	0.16	0.02
S	2408	1296	2482	1750	-230	-234	460	44
p-value	0	0	0	0	0.31	0.31	0.04	0.85
Significance	**	**	**	**	ns	ns	*	ns

*** indicates highly significant, * indicates significant and ns means non-significant trend*

Estimation of sediment yield with the wettest climate scenario

Temporal analysis

The temporal distribution of sediment yield of the watershed in both RCPs is presented in (Figure 11).

In RCP 4.5, the sediment yields for the study watershed ranged from 0.2 t ha⁻¹ yr⁻¹ to 71.5 t ha⁻¹ yr⁻¹ with the average of 13.7 t ha⁻¹. Six years were determined to be the most problematic years, with an average yearly sediment of more than 30 t ha⁻¹. The average sediment yield of the watershed in the near future (2022-2060) was 16 t ha⁻¹ yr⁻¹, which was found to be higher than the far future average of 11.6 t ha⁻¹ yr⁻¹.

In RCP 8.5, the simulated average sediment from the watershed was ranged from 0.2 t ha⁻¹ and 82.3 t ha⁻¹ with the average of 16.1 t ha⁻¹ yr⁻¹. The near (2022-2060) and far (2061-2098) future annual sediment loss of the watershed was projected to be 10.5 t ha⁻¹ yr⁻¹ and 21.6 t ha⁻¹ yr⁻¹, respectively. This demonstrated that the average sediment yield in the far future will increase by 20.4% relative to the baseline average sediment. The far future sediment loss in the watershed showed an increase of 11.1 t ha⁻¹ yr⁻¹ over the preceding estimate near future average sediment loss. This demonstrated that, in comparison to the average sediment yield of the near future, the sediment yield will double toward the end of the century.

It was discovered that, in comparison to the baseline sediment, the near future (2022–2060) sediment was equal to it in RCP 4.5 and decreased by 41% in RCP 8.5, whereas the far future (2061–2098) sediment grew by 20.4% in RCP 8.5 and decreased by 35% in RCP 4.5. Out of the projected 76 years, 21 and 23 years shown positive deviations from the mean of the existing sediment yield under RCP 4.5 and 8.5, respectively. The graph below (Figure 11) makes it quite evident that the trend of sediment yield in RCP 4.5 is declining while it is rising in RCP 8.5. In this climatic scenario, 42 (in RCP 4.5) and 44 (in RCP 8.5) years out of the projected 76 years were found to be susceptible to sediment loss. The annual sediment yield of the watershed is determined to be over the threshold level (10 t ha⁻¹) of the country's highland region, although the proportionate change of most of the years in both RCPs was negative. This can be attributed to the watershed's high susceptibility to sediment yield since the baseline.

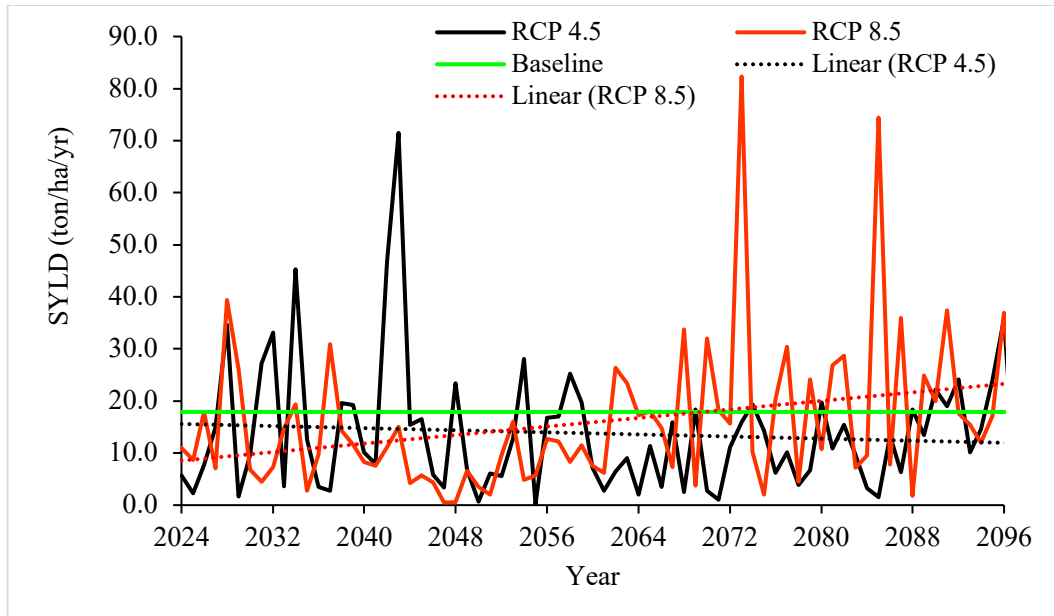


Figure 11 - Temporal variability of sediment yields as simulated using the wettest climate model

Spatial analysis

The spatial variability of sediment yield in both RCPs is illustrated in (Figure 12). The near future annual sediment yield ranged from 0.33 to 46.7 t ha⁻¹. Similarly, the far future sediment ranged from 0.22 to 32.51 t ha⁻¹. Sub-basins 20, 25, and 13 were the watershed's safest sub-basins losing less than one t ha⁻¹ yr⁻¹, while sub-basins 24 and 14 are the most susceptible, losing an average of more than 30 t ha⁻¹ yr⁻¹. However, most of the sub-basins (18 sub-basins and 17 sub-basins in the near and far future, respectively) were found to be vulnerable to sediment loss above the tolerable soil loss limit proposed for the Ethiopia highlands. Generally, northern, eastern, and southwestern regions of the watershed were identified to be vulnerable to sediment loss.

In RCP 8.5, sub-basins 14 and 25 experienced the highest and lowest sediment loss, respectively. Furthermore, it was found that sediment loss might occur in both time frames in sub-basins that were found to be vulnerable in RCP 4.5 and that were situated in the watershed's northern, eastern, and western areas. In contrast, sub-basins in the Northwestern and Southern areas lost only a little quantity of sediment and were considered safe basins (Figure 12).

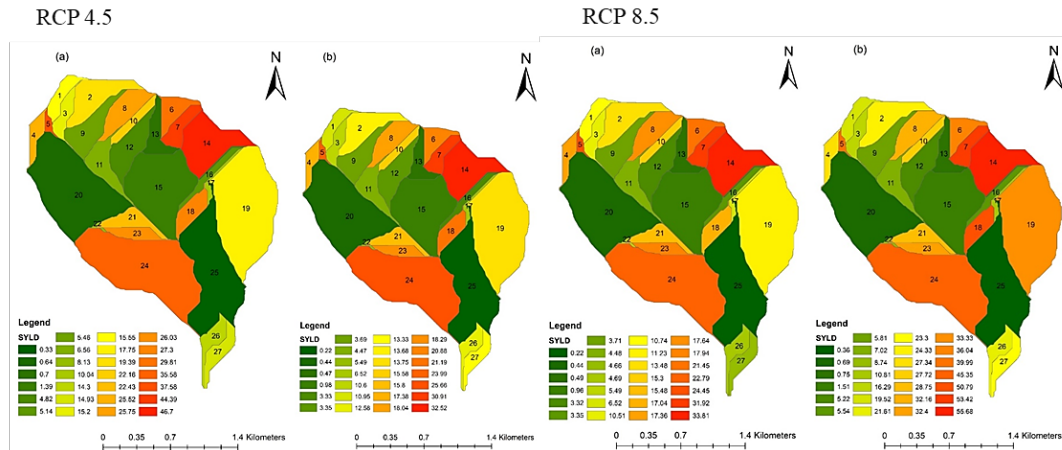


Figure 12 - The spatial distribution of the projected sediment yield ($t\ ha^{-1}\ yr^{-1}$) from the wettest climate model (CCCma (CRCM4) and SWAT for the years (a) 2022-2060 and (b) 2061-2098.

Estimation of sediment yield with the driest climate model

Temporal analysis

The average sediment yield of the watershed in both RCPs of this driest climate scenario is presented in (Figure 13).

In RCP 4.5, the sediment yield of the watershed is estimated to be $4.7\ t\ ha^{-1}\ yr^{-1}$. Sediment yields for the study watershed varied through time, ranging from $0.04\ t\ ha^{-1}\ yr^{-1}$ to $16.1\ t\ ha^{-1}\ yr^{-1}$ in 2065 and 2025, respectively. Five years were determined with an average annual sediment yield of more than the tolerable soil loss limit for Ethiopia highlands ($10\ t\ ha^{-1}$). These years were 2042, 2046, 2065, 2076, and 2077 and the annual sediment loss for each was 16.1, 10.4, 10.8, 14.4, and $10.04\ t\ ha^{-1}\ yr^{-1}$, respectively. The average sediment yield of the watershed in the near future was projected to be $6.6\ t\ ha^{-1}\ yr^{-1}$, which is almost twice the average sediment yield in the far future ($3.5\ t\ ha^{-1}\ yr^{-1}$).

The projected average sediment yield in RCP 8.5 of the watersheds is estimated to be $4.06\ t\ ha^{-1}\ yr^{-1}$. The sediment yield of the study watershed varied through time, ranging from $0.275\ t\ ha^{-1}\ yr^{-1}$ to $11.8\ t\ ha^{-1}\ yr^{-1}$ in 2033 and 2098, respectively. Six years were identified with an average yearly sediment loss of more than $10\ t\ ha^{-1}$. These years were 2024, 2030, 2032, 2057, 2059, and 2098 and the annual sediment loss for each was 10.3, 11.4, 10.89, 11.79, 11.11, and $11.8\ t\ ha^{-1}\ yr^{-1}$, respectively. The average sediment yield of the watershed in the near future is projected to be $4.16\ t\ ha^{-1}\ yr^{-1}$, which was higher than the average of the far future ($3.97\ t\ ha^{-1}\ yr^{-1}$). The temporal distribution of sediment yield under this RCP is comparable with RCP 4.5.

In this driest climatic scenario, the sediment production was generally lower than in the baseline. Conversely, comparable trends to the wettest climate model were discovered; the tendency indicates that sediment yield will decrease in RCP 4.5 and increase in RCP 8.5 when it goes towards the end of this century, as shown in the graph below (Figure 13).

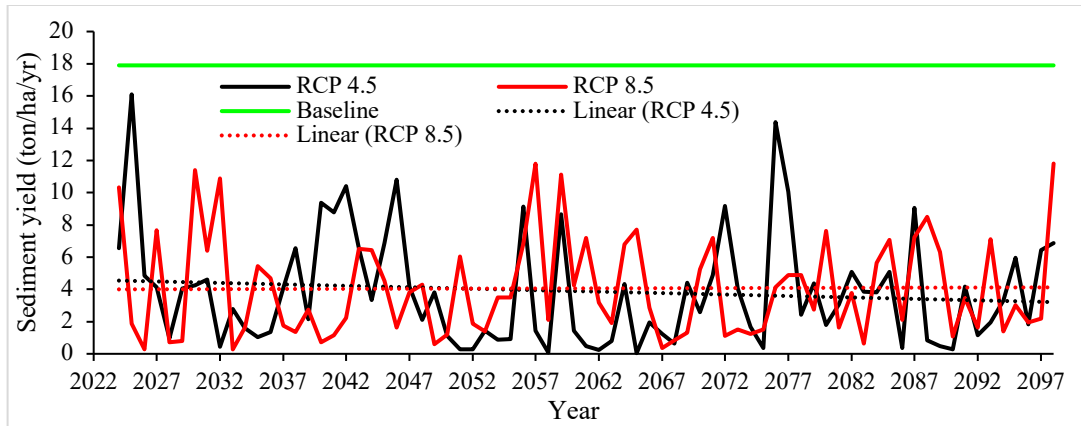


Figure 13 - Temporal distributions of sediment yield as simulated from the driest climate model (MPI (RCA4))

Spatial analysis

The spatial distribution of sediment yield in both RCPs is presented in (Figure 14).

In RCP 4.5, sub-basins 14 and 25 experienced the highest and lowest sediment yield, respectively. The range of sediment yield was from $0.11 \text{ t ha}^{-1} \text{ yr}^{-1}$ to $13.6 \text{ t ha}^{-1} \text{ yr}^{-1}$ in the near future and from 0.08 to $12.8 \text{ t ha}^{-1} \text{ yr}^{-1}$ in the far future. This showed that there was not a major change in the sediment yield of the watershed with time. Additionally, it was determined that sub-basins found in the Northern, Eastern, and Western regions of the watershed were susceptible to sediment loss in both time frames. While sub-basins found in Northwestern and Southern regions were deemed to be safe basins; they contributed a modest amount of sediment.

In RCP 8.5, the sediment yield results demonstrated that the watershed's southwestern, northern, and eastern regions are more prone to erosion than its northwestern and central regions. Sub-basins found in the eastern part of the watershed are suffering from the highest sediment loss, and in the reverse: sub-basins with comparatively high runoff in the central part of the watershed are less vulnerable to sediment loss. This showed that even when the watershed has high runoff, the runoff does not always contain sediment and that the area of the watershed where little runoff occurs does not always have pure water.

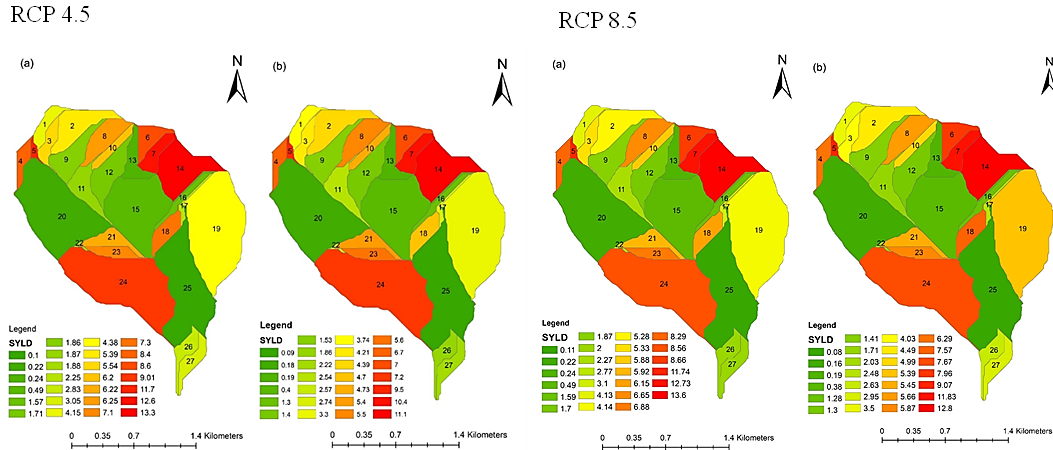


Figure 14 - The spatial distribution of projected sediment yield ($t\ ha^{-1}\ yr^{-1}$) from the driest climatic model MPI (RCA4) (RCP 4.5) and SWAT for the years (a) 2022-2060, and (b) 2061-2098.

Discussion

The capability of SWAT to simulate sediment

The finding of this study confirmed that SWAT could simulate the sediment yield of the study watershed. The simulation result was evaluated using objective functions and the model was found to be reliable and accurate. Similarly, the SWAT model can predict sediment yields in Fincha Watershed, Ethiopia with $R^2 = 0.82$ and $ENS = 0.80$ during the calibration period and $R^2 = 0.80$ and $ENS = 0.78$ during the validation period (Ayana et al., 2012). The SWAT model reasonably simulated the sediment yield with R^2 of 0.78 and R^2 of 0.84 (Getinet, 2021), R^2 of 0.85 and R^2 of 0.77 (Gebremariam, 2019) for calibration and validation, respectively. Studies in similar watersheds reported, simulated and observed sediment yield was found to be significantly correlated (Gebrie, 2018; Lebay, 2022 and Ashagre, 2009).

Estimation of sediment yield with SWAT

The study described that the watershed was losing sediment greater than the proposed soil loss limit of the Ethiopian highland. The tolerable soil loss that can maintain the economy and a high level of production ranges from 5 to 11 $t\ ha^{-1}\ yr^{-1}$ (Husen and Abate, 2020; Libourel, 2014; Renard et al., 1997), while the average sediment yield of the study watershed was 17.9 $t\ ha^{-1}\ yr^{-1}$. The spatial distributions of the sediment yield showed that 17 sub-basins have high sediment yields among the 27 sub-basins generated by the SWAT model. Each sub-basin has a different sediment yield due to the land use system, slope, and other influencing factors. The majority of these vulnerable sub-basins are found in the northeastern, western, and eastern parts of the watershed on agricultural land that has active gullies and a slope class of 20% to 30%. While sub-basins located in the central regions of the watershed were terraced and were less vulnerable to sediment loss.

According to the climatic and biophysical characteristics of their study area, other studies of similar nature carried out in numerous regions of Ethiopia and elsewhere in the world

found varying results for sediment yield. Similar research in the Upper Blue Nile Basin calibrated for the years 1992 to 2020 estimated that the watershed's mean annual sediment yield was $17.9 \text{ t ha}^{-1} \text{ yr}^{-1}$ (Abebe et al., 2022). Another study conducted in Anjeni also found yearly average sediment yields of 27.8 t ha^{-1} (Setegn et al., 2010). A comparable study carried out in the Gumara Maksegnit watershed found an average yearly sediment yield of 21.08 Mg/hm^2 , which is far higher than the potential rate of soil regeneration (Addis et al., 2016). In another study conducted using the SWAT model in the Kesem Dam, A wash basin reported the mean annual sediment yield of the watershed was $11.43 \text{ t ha}^{-1} \text{ yr}^{-1}$ (Abebe and Tolessa, 2020). The study carried out in the Xinjiang River Basin reported that the annual sediment yield rate ranged from $3 \text{ t ha}^{-1} \text{ yr}^{-1}$ in riparian lowlands to $33 \text{ t ha}^{-1} \text{ yr}^{-1}$ in the mountain highlands, with a mean of $19 \text{ t ha}^{-1} \text{ yr}^{-1}$ in the basin (Yuan and Forshay, 2020b). In contrast, the study reported the total annual average sediment yield for the entire Blue Nile Basin is $4.26 \text{ t ha}^{-1} \text{ yr}^{-1}$ (Fetene et al., 2008).

Sediment yield with future climatic scenarios

The analysis of both the driest and wettest climate scenarios reveals a definitive rise in temperature alongside an unclear trend in rainfall patterns. This temperature increase, irrespective of the precipitation trends, has significant implications for sediment yield in the studied watershed. Under the driest climatic models, there is a notable reduction in sediment yield compared to the current rate, which suggests that lower moisture availability might limit soil erosion processes. However, it is important to highlight that despite this overall reduction, five out of the 76 years of the projection period exhibited sediment loss exceeding the tolerable soil loss limit characteristic of the Ethiopian highlands.

In a more detailed analysis of the sediment loss projections under both RCPs, the study identified that out of the 76 projected years, 42 years under RCP 4.5 and 44 years under RCP 8.5 experienced sediment loss above the tolerable limit. This indicates that while the overall trend might suggest a decrease in sediment yield under the driest scenarios, the frequency of extreme soil loss events remains significant and even more prevalent under higher emission scenarios (RCP 8.5).

Supporting evidence from other studies reinforces these findings. For instance, Girmay et al. (2021) found that the soil loss rate is anticipated to increase under both RCP 4.5 and RCP 8.5 scenarios. This suggests that the expected rise in temperature and potential changes in rainfall intensity will enhance the erosive power of rainfall, leading to greater soil loss. Additionally, Belay and Mengistu (2021) indicated that the middle of this century could witness an increase in soil erosion rates compared to the baseline period due to the greater erosive potential of rainfall driven by climate change.

These findings underscore the complex interplay between climate change variables and soil erosion processes. While reduced moisture availability in drier scenarios might limit sediment yield on average, the increased temperature and potential for more intense rainfall events could offset these benefits, leading to significant soil erosion in specific years. The higher frequency of extreme erosion events under RCP 4.5 and RCP 8.5 highlights the need for targeted soil conservation strategies to mitigate the adverse impacts of climate change on soil erosion. This nuanced understanding of sediment yield dynamics is crucial for developing effective climate adaptation and mitigation plans. Gadissa et al. (2018) reported that the rate of sedimentation in Lake Ziway will drop by 38% under RCP4.5 and by 23%

under RCP8.5. This reduction is attributed to the anticipated decrease in rainfall and increase in temperature, which might reduce runoff and, consequently, sediment transport to the lake.

The other finding stated, that in comparison to the baseline period, climate change is predicted to increase average annual sediment yield by 4% to 32% (Zhang et al., 2019). This significant range underscores the variability and uncertainty inherent in climate projections and their impact on sediment dynamics. By the 2030s and 2060s, the climatic variable increments were predicted to cause intensifications in the mean annual sediment yield of 4.42% and 8.08% for RCP 4.5 and 7.19% and 10.79% for RCP 8.5 (Jilo et al., 2019). These figures suggest a clear trend of increasing sediment yield over time, with more pronounced effects under higher emission scenarios.

Furthermore, projections for mean annual stream flow also indicate substantial increases due to climate variables. For 2020, 2050, and 2080s, the increases in climate variables are predicted to increase mean annual stream flow by 8%, 13%, and 15% for the RCP2.6 scenario, 17%, 24%, and 31% for the RCP4.5 scenario, and 14%, 24%, and 35% for the RCP8.5 scenario; this, in turn, increases sediment yield (Mohammed, 2020). These findings illustrate how changes in precipitation and temperature patterns will likely exacerbate erosion processes, leading to higher sediment yields. Similar findings reported that climate change could increase sediment yield by up to 10% per year if not controlled (Theron et al., 2021). This highlights the urgency of implementing effective soil conservation measures to mitigate the adverse effects of increased erosion and sedimentation.

The projected increases in sediment yield under various RCP scenarios indicate a significant potential for enhanced soil erosion, driven by changes in rainfall intensity and increased temperatures. However, specific cases like Lake Ziway highlight the complex interplay between climatic factors and local geography, suggesting that the impacts of climate change on sediment dynamics can vary widely.

Conclusion and Recommendations

This research provides valuable insights into the spatiotemporal distribution of sediment yield in the Andit Tid watershed under current and projected climatic scenarios. Using SWAT and Arc GIS 10.5, the study estimated an annual average sediment yield of $17.9 \text{ t ha}^{-1} \text{ yr}^{-1}$, with calibration and validation R^2 values of 0.62 and 0.72, respectively. Future projections indicate variability in sediment yield depending on the climatic scenario, with significant differences observed between RCP 4.5 and RCP 8.5 pathways. Notably, the watershed's northeastern, eastern, and western regions, primarily steeply sloped farmland with active gullies, were identified as major contributors to sediment yield.

It is advised that targeted management techniques be implemented using the spatiotemporal distribution maps generated by this study. Provide priority to interventions in areas designated as hotspots for sediment yield, particularly in the eastern, western, and northeastern regions which are marked by active gullies and steep slopes. Adaptation strategies that consider the predicted changes in sediment yields under varied climatic scenarios; in particular, there should be a focus on emission mitigation to prevent the higher sediment yields predicted under RCP 8.5.

Acknowledgments

The authors would like to acknowledge the Amhara Regional Agricultural Research Institute (ARARI), Makerere University, German Academic Exchange Service (DAAD), and Water and Land Resource Center (WLRC) for their cooperation and support during the whole life of this research. We also would like to thank Mr. Tilahun Getachew, Mr. Getacher Kassa, Mr. Kebede Bekele, Mr. Temesgen Yilma, Mr. Solomon Alemu, and Mr. Amare Belachew for their help during data collection and encoding.

References

- Abbaspour, K. C. (2015). *SWAT-CUP: SWAT Calibration and Uncertainty programs-A user manual* (pp. 1–100).
- Abebe, B. K., Zimale, F. A., Gelaye, K. K., Gashaw, T., Dagnaw, E. G., & Adem, A. A. (2022). Application of Hydrological and Sediment Modeling with Limited Data in the Upper Blue Nile Basin, Ethiopia. *Hydrology*, 9(10), 167. <https://doi.org/10.3390/hydrology9100167>
- Abebe, T., & Gebremariam, B. (2019). Modeling runoff and sediment yield of Kesem dam watershed, Awash basin, Ethiopia. *SN Applied Sciences*, 1(5). <https://doi.org/10.1007/s42452-019-0347-1>
- Abebe, T., & Tolessa, O. (2020). Sediment Yield Estimation and Effect of Management Options on Sediment Yield of Kesem Dam Watershed , Awash Basin , Ethiopia. *Scientific African*, 9, e00425. <https://doi.org/10.1016/j.sciaf.2020.e00425>
- Addis, H. K., Strohmeier, S., Ziadat, F., Melaku, N. D., & Klik, A. (2016). Modeling streamflow and sediment using SWAT in ethiopian highlands. *International Journal of Agricultural and Biological Engineering*, 9(5), 51–66. <https://doi.org/10.3965/j.ijabe.20160905.2483>
- Admas, M., Melesse, A. M., Abate, B., & Tegegne, G. (2022). Soil Erosion , Sediment Yield , and Runoff Modeling of the Megech Watershed Using the GeoWEPP Model. *Hydrology*, 9, 208.
- Aduugna, A. (2015). Soil erosion assessment and control in Northeast Wollega, Ethiopia. *Solid Earth Discussions*, 7(4), 3511–3540. <https://doi.org/10.5194/sed-7-3511-2015>
- Amsalu, A., & de Graaff, J. (2006). Farmers' views of soil erosion problems and their conservation knowledge at Beressa watershed, central highlands of Ethiopia. *Agriculture and Human Values*, 23(1), 99–108. <https://doi.org/10.1007/s10460-005-5872-4>
- Ashagre, B. B. (2009). *SWAT TO IDENTIFY WATERSHED MANAGEMENT OPTIONS: (ANJENI WATERSHED, BLUE NILE BASIN, ETHIOPIA)*. Presented to the Faculty of the Graduate School of Cornell University.
- Ayana, A. B., Edossa, D. C., & Kositsakulchai, E. (2012). Simulation of sediment yield using SWAT model in Fincha watershed, Ethiopia. *Kasetsart Journal - Natural Science*, 46(2), 283–297.
- Ayele, H. S., Li, M. H., Tung, C. P., & Liu, T. M. (2016). Impact of Climate Change on Runoff in the Gilgel Abbay Watershed, the Upper Blue Nile Basin, Ethiopia. *Water (Switzerland)*, 8(9). <https://doi.org/10.3390/w8090380>
- Balabathina, V. N., Raju, R. P., Muluaalem, W., & Tadele, G. (2020). Estimation of soil loss using remote sensing and GIS-based universal soil loss equation in northern catchment

- of Lake Tana Sub-basin, Upper Blue Nile Basin, Northwest Ethiopia. *Environmental Systems Research*, 9(1). <https://doi.org/10.1186/s40068-020-00203-3>
- Bayabil, H. K., & Dile, Y. T. (2020). Improving hydrologic simulations of a small watershed through soil data integration. *Water (Switzerland)*, 12(10). <https://doi.org/10.3390/w12102763>
- Belay, T., & Mengistu, D. A. (2021). Impacts of land use/land cover and climate changes on soil erosion in Muga watershed, Upper Blue Nile basin (Abay), Ethiopia. *Ecological Processes*, 10(1). <https://doi.org/10.1186/s13717-021-00339-9>
- Belayneh, M., Yirgu, T., & Tsegaye, D. (2020). Runoff and soil loss responses of cultivated land managed with graded soil bunds of different ages in the Upper Blue Nile basin, Ethiopia. *Ecological Processes*, 9(1). <https://doi.org/10.1186/s13717-020-00270-5>
- Betrie, G. D., Mohamed, Y. A., Van Griensven, A., & Srinivasan, R. (2011). Sediment management modelling in the Blue Nile Basin using SWAT model. *Hydrology and Earth System Sciences*, 15(3), 807–818. <https://doi.org/10.5194/hess-15-807-2011>
- Bieger, K., Arnold, J. G., Rathjens, H., White, M. J., Bosch, D. D., Allen, P. M., Volk, M., & Srinivasan, R. (2017). Introduction to SWAT+, A Completely Restructured Version of the Soil and Water Assessment Tool. *Journal of the American Water Resources Association*, 53(1), 115–130. <https://doi.org/10.1111/1752-1688.12482>
- Binbin Zhang, Narayan Kumar Shrestha, Prasad Daggupati, Ramesh Rudra, Rituraj Shukla, B. K. and J. H. (2018). Quantifying the impacts of climate change on streamflow dynamics of two major rivers of the Northern Lake Erie basin in Canada. *Sustainability*, 10(8), 2897. <https://doi.org/doi:10.3390/su10082897>
- Boskidis, I., Gikas, G. D., Sylaios, G. K., & Tsihrintzis, V. A. (2012). Hydrologic and Water Quality Modeling of Lower Nestos River Basin. *Water Resources Management*, 26(10), 3023–3051. <https://doi.org/10.1007/s11269-012-0064-7>
- Burn, D., Cunderlik, J., Pietroniro, A. (2004). Hydrological trends and variability in the Liard River basin. *Hydrol. Sci. J.*, 49, 53–68.
- D. N. Moriasi, J. G. Arnold, M. W. Van Liew, R. L. Bingner, R. D. Harmel, & T. L. Veith. (2007). Model Evaluation Guidelines for Systematic Quantification of Accuracy in Watershed Simulations. *Transactions of the ASABE*, 50(3), 885–900. <https://doi.org/10.13031/2013.23153>
- Dakhlalla, A. O., & Parajuli, P. B. (2019). Assessing model parameters sensitivity and uncertainty of streamflow, sediment, and nutrient transport using SWAT. *Information Processing in Agriculture*, 6(1), 61–72. <https://doi.org/10.1016/j.inpa.2018.08.007>
- Daniel, M., Woldeamlak, B., Lal, R. (2014). Recent spatiotemporal temperature and rainfall variability and trends over the upper Blue Nile river basin, Ethiopia. *Int. J. Climatol.*, 34(2278–2292).
- Daniel Mengistu, Woldeamlak Bewket, and R. L. (2015). Soil Erosion Hazard Under the Current and Potential Climate Change Induced Loss of Soil Organic Matter in the Upper Blue Nile (Abay) River Basin, Ethiopia. In *Sustainable Intensification to Advance Food Security and Enhance Climate Resilience in Africa* (Issue December 2017, pp. 137–162). <https://doi.org/10.1007/978-3-319-09360-4>
- Das, B., Jain, S., Singh, S., & Thakur, P. (2019). Evaluation of multisite performance of SWAT model in the Gomti River Basin, India. *Applied Water Science*, 9(5), 1–10. <https://doi.org/10.1007/s13201-019-1013-x>
- Essenfelder, A. H. (2016). *Weather Database: a quick guide* (Issue March).

- Fetene, F., Awulachew, S. B., & Teklie, N. (2008). Development of Rainfall-Runoff-Sediment Discharge Relationship in the Blue Nile Basin. *Development of Rainfall-Runoff-Sediment Discharge Relationship in the Blue Nile Basin*, 112–131.
- G. W. Feyereisen, T. C. Strickland, D. D. Bosch, & D. G. Sullivan. (2007). Evaluation of SWAT Manual Calibration and Input Parameter Sensitivity in the Little River Watershed. *Transactions of the ASABE*, 50(3), 843–855. <https://doi.org/10.13031/2013.23149>
- Gadissa, T., Nyadawa, M., Behulu, F., & Mutua, B. (2018). The Effect of Climate Change on Loss of Lake Volume : Case of Sedimentation in Central Rift Valley. *Hydrology*, 5(67), 1–18. <https://doi.org/10.3390/hydrology5040067>
- Gebrie, T. (2018). *Sediment Yield Modeling of Dedissa Sub Basin , Abay Basin , South-Western Sediment Yield Modeling of Dedissa Sub Basin , Abay Basin ,. September*, 120–127.
- George H. Hargreaves, & Zohrab A. Samani. (1985). Reference Crop Evapotranspiration from Temperature. *Applied Engineering in Agriculture*, 1(2), 1–12. <https://doi.org/10.13031/2013.26773>
- Getaneh Ayele, B., Woldemariam, A. D., & Addis, H. K. (2024). Validation of CORDEX Regional climate models to simulate climate trends and variability across various agro-ecological zones of North Shewa, Ethiopia. *Water-Energy Nexus*, 7, 87–102. <https://doi.org/10.1016/j.wen.2024.01.001>
- Getinet, A. (2021). *Runoff and Sediment Yield Simulation in the Weyib watershed, Genale Dawa Basin, MSc thesis Addis Abeba University, Ethiopia*.
- Girmay, G., Moges, A., & Muluneh, A. (2021). Assessment of Current and Future Climate Change Impact on Soil Loss Rate of Agewmariam Watershed, Northern Ethiopia. *Air, Soil and Water Research*, 14. <https://doi.org/10.1177/1178622121995847>
- Gupta, H.V.; Kling, H.; Yilmaz, K.K.; Martinez, G. F. (2009). Decomposition of the mean squared error and NSE performance criteria: Implications for improving hydrological modelling. *J. Hydrol*, 377, 80–91.
- Gupta HV, Beven KJ, W. T. (2006). Model calibration and uncertainty estimation. In *Encyclopedia of hydrological sciences* (pp. 11–131).
- Gupta HV, Sorooshian S, Y. P. (1999). Status of automatic calibration for hydrologic models: comparison with multilevel expert calibration. *J Hydrol Eng*, 4(2), 135–143.
- Hassan, A. (2012). *Eastern Nile Planning Model (ENPM) Project*.
- Hawando, T. (1997). *Desertification in Ethiopian Highlands*.
- Hurni, H. (1988). Climate, Soil, and Water: Degradation and Conservation of the Resources in the Ethiopian Highlands. *Mountain Research and Development*, 8(123–130).
- Hurni, H. (1993). Land degradation, famine, and land resource scenarios in Ethiopia. In *World soil erosion and conservation*. <https://doi.org/10.1017/cbo9780511735394.004>
- Husen, D., & Abate, B. (2020). Estimation of Runoff and Sediment Yield Using SWAT Model: The Case of Katar Watershed, Rift Valley Lake Basin of Ethiopia. *International Journal of Mechanical Engineering and Applications*, 8(6), 125. <https://doi.org/10.11648/j.ijmea.20200806.11>
- IAEA. (2014). Assessment of soil erosion and sedimentation: the role of fallout radionuclides. In *Guidelines for Using Fallout Radionuclides to Assess Erosion and Effectiveness of Soil Conservation Strategies, IAEA-TECDOC-1741, IAEA, Vienna*.

- Izzaddin, A., Langousis, A., Totaro, V., Yaseen, M., & Iacobellis, V. (2024). A new diagram for performance evaluation of complex models. *Stochastic Environmental Research and Risk Assessment*, 38(6), 2261–2281. <https://doi.org/10.1007/s00477-024-02678-3>
- J.G. Arnold, J.R. Kiniry, R. Srinivasan, J.R. Williams, E.B. Haney, S. L. N. (2011). Soil and Water Assessment Tool Input/Output File Documentation Version 2009. In *Soil and Water Assessment Tool* (Issue December).
- Jilo, N. B., Gebremariam, B., Harka, A. E., Woldemariam, G. W., & Behulu, F. (2019). Evaluation of the impacts of climate change on sediment yield from the Logiya Watershed, Lower Awash Basin, Ethiopia. *Hydrology*, 6(3). <https://doi.org/10.3390/hydrology6030081>
- Kefyalew Tilahun, E. (2021). Cause and cost of onsite nutrient loss replacement in the highlands of Ethiopia and implication of Soil and Water Conservation measures. *International Journal of Agricultural Science and Food Technology*, 7, 154–163. <https://doi.org/10.17352/2455-815x.000103>
- Kendall, M. G. (1975). *Rank Correlation Methods*, 4th ed. Charles Griffin, London.
- Khanal, S., & Parajuli, P. B. (2014). Sensitivity Analysis and Evaluation of Forest Biomass Production Potential Using SWAT Model. *Journal of Sustainable Bioenergy Systems*, 04(02), 136–147. <https://doi.org/10.4236/jsbs.2014.42013>
- Kondolf, G. M., Gao, Y., Annandale, G. W., Morris, G. L., Jiang, E., Zhang, J., Cao, Y., Carling, P., Fu, K., Guo, Q., Hotchkiss, R., Peteuil, C., Sumi, T., Wang, H., Wang, Z., Wei, Z., Wu, B., Wu, C., & Yang, C. T. (2014). Sustainable sediment management in reservoirs and regulated rivers: Experiences from five continents. *Earth's Future*, 2(5), 256–280. <https://doi.org/10.1002/2013ef000184>
- Krause, P., Boyle, D. P., & Bäse, F. (2005). Comparison of different efficiency criteria for hydrological model assessment. *Advances in Geosciences*, 5, 89–97. <https://doi.org/10.5194/adgeo-5-89-2005>
- Legates, David R., B. aton R., & Jr., G. J. M. (1999). Evaluating the use of goodness-of-fit Measures in hydrologic and hydroclimatic model validation. *WATER RESOURCES RESEARCH*, 35(1), 233–241.
- Leta, M. K., Demissie, T. A., & Tränckner, J. (2021). Modeling and prediction of land use land cover change dynamics based on land change modeler (Lcm) in nashe watershed, upper blue Nile basin, Ethiopia. *Sustainability (Switzerland)*, 13(7). <https://doi.org/10.3390/su13073740>
- Libourel, É. (2014). Géographies de Fernand VERGER : l'environnement comme horizon. *Physio-Géo, Volume 8*, 1–52. <https://doi.org/10.4000/physio-geo.4082>
- M.A. Nearing, F.F. Pruski, and M. R. O. (2004). Expected climate change impacts on soil erosion rates: A review. *Journal of Soil and Water Conservation*, 59(1), 43–50.
- McCuen, R. H., Knight, Z., & Cutter, A. G. (2006). Evaluation of the Nash–Sutcliffe Efficiency Index. *Journal of Hydrologic Engineering*, 11(6), 597–602. [https://doi.org/10.1061/\(asce\)1084-0699\(2006\)11:6\(597\)](https://doi.org/10.1061/(asce)1084-0699(2006)11:6(597))
- Mekin Mohammed, B. B. and M. D. B. (2020). Hydrological Impacts of Climate Change in Tikur Wuha Watershed, Ethiopian Rift Valley Basin. *Journal of Environment and Earth Science*, 10(2). <https://doi.org/10.7176/jees/10-2-04>
- Mengie Belayneh, Teshome Yirgu, and D. T. (2019). *Potential soil erosion estimation and area prioritization for better conservation planning in Gumara watershed using RUSLE and GIS technique*. Mettu University, Ethiopia.

- Mengistu, A. G., van Rensburg, L. D., & Woyessa, Y. E. (2019). Techniques for calibration and validation of SWAT model in data scarce arid and semi-arid catchments in South Africa. *Journal of Hydrology: Regional Studies*, 25, 1–18. <https://doi.org/10.1016/j.ejrh.2019.100621>
- Mengistu, D., Bewket, W., & Lal, R. (2012). Soil Erosion Hazard Under the Current and Potential Climate Change Induced Loss of Soil Organic Matter in the Upper Blue Nile (Abay) River Basin, Ethiopia. In *Sustainable Intensification to Advance Food Security and Enhance Climate Resilience in Africa* (Issue December 2012). <https://doi.org/10.1007/978-3-319-09360-4>
- Meresa, H. K., & Gatachew, M. T. (2019). Climate change impact on river flow extremes in the upper blue Nile river basin. *Journal of Water and Climate Change*, 10(4), 759–781. <https://doi.org/10.2166/wcc.2018.154>
- Moges, D. M., Knoch, A., Bhat, H. G., & Uemaa, E. (2020). Future soil loss in highland Ethiopia under changing climate and land use. *Regional Environmental Change*, 20(1), 1–14. <https://doi.org/10.1007/s10113-020-01617-6>
- MULUKEN LEBAY. (2022). *RESPONSE OF DISCHARGE AND SEDIMENT YIELD TO MANAGEMENT OPTIONS AND CLIMATE CHANGE SCENARIOS IN MAYBAR SUB-WATERSHED, SOUTH WOLLO ZONE, ETHIOPIA* [Hawassa University]. <https://www.who.int/news-room/fact-sheets/detail/autism-spectrum-disorders>
- Nash, J. E. ; S. J. V. (1970). River flow forecasting through conceptual models. Part I. A discussion of principles. *J Hydrol*, 10(3), 282–290.
- NMA. (2007). *Climate Change National Adaptation Programme of Action (NAPA) of Ethiopia, Addis Ababa, Ethiopia*.
- Orke, Y. A., & Li, M. (2022). Impact of Climate Change on Hydrometeorology and Droughts in the Bilate Watershed , Ethiopia. *Water*, 14(729), 1–31.
- R, A., Ahrends, H., Habib-Ur-rahman, M., & Gaiser, T. (2021). Modeling approaches to assess soil erosion by water at the field scale with special emphasis on heterogeneity of soils and crops. *Land*, 10(4), 422. <https://doi.org/10.3390/land10040422>
- Rathjens, H.; Bieger, K.; Srinivasan, R.; Arnold, J. G. (2016). *CMhyd User Manual Documentation for Preparing Simulated Climate Change Data for Hydrologic Impact Studies*.
- Renard, K., Foster, G., Weesies, G., McCool, D. and Yoder, D. (1997). *Predicting Soil Erosion by Water: A Guide to Conservation Planning with the Revised Universal Soil Loss Equation (RUSLE)*. US Department of Agriculture, Agriculture Handbook No.703USDA, USDA, Washington DC.
- Reungsang, P., Kanwar, R. S., Jha, M., Gassman, P. W., Ahmad, K., & Saleh, A. (2007). Calibration and validation of SWAT for the upper maquoketa river watershed. In *International Agricultural Engineering Journal* (Vol. 16, Issues 1–2).
- Roth, V., Nigussie, T. K., & Lemann, T. (2016). Model parameter transfer for streamflow and sediment loss prediction with SWAT in a tropical watershed. *Environmental Earth Sciences*, 75(19). <https://doi.org/10.1007/s12665-016-6129-9>
- S.L. NEITSCH, J.G. ARNOLD, J.R. KINIRY, J. R. W. (2005). Soil and Water Assessment Tool Documentation. In *SWAT user manual*.
- Sa'adi, Z., Shahid, S., Chung, E. S., & Ismail, T. bin. (2017). Projection of spatial and temporal changes of rainfall in Sarawak of Borneo Island using statistical downscaling of CMIP5 models. *Atmospheric Research*, 197(February), 446–460. <https://doi.org/10.1016/j.atmosres.2017.08.002>

- Saha, P. P., Zeleke, K., & Hafeez, M. (2014). Streamflow modeling in a fluctuant climate using SWAT: Yass River catchment in south eastern Australia. *Environmental Earth Sciences*, 71(12), 5241–5254. <https://doi.org/10.1007/s12665-013-2926-6>
- School J, A. K. (2007). Using monthly weather statistics to generate daily data in a SWAT model application to West Africa. *Ecol Model*, 201(3–4), 301–311.
- Setegn, S. G., Dargahi, B., Srinivasan, R., & Melesse, A. M. (2010). Modeling of sediment yield from anjeni-gauged watershed, Ethiopia using swat model1. *Journal of the American Water Resources Association*, 46(3), 514–526. <https://doi.org/10.1111/j.1752-1688.2010.00431.x>
- Setegn, S. G., Srinivasan, R., & Dargahi, B. (2008). Hydrological Modelling in the Lake Tana Basin, Ethiopia Using SWAT Model. *The Open Hydrology Journal*, 2(1), 49–62. <https://doi.org/10.2174/1874378100802010049>
- Shiferaw, B. and Holden, S. (1999). Soil Erosion and Smallholders' Conservation Decisions in the Highlands of Ethiopia. *World Development*, 27(4), 739–752.
- Shrestha, B., Cochrane, T. A., Caruso, B. S., Arias, M. E., & Piman, T. (2016). Uncertainty in flow and sediment projections due to future climate scenarios for the 3S Rivers in the Mekong Basin. *Journal of Hydrology*, 540, 1088–1104. <https://doi.org/10.1016/j.jhydrol.2016.07.019>
- Smith, E. D., Szidarovszky, F., Karnavas, W. J., & Bahill, A. T. (2008). Sensitivity Analysis, a Powerful System Validation Technique. *The Open Cybernetics & Systemics Journal*, 2(1), 39–56. <https://doi.org/10.2174/1874110x00802010039>
- SUTCLIFFE, J. E. N. and I. V. (1970). RIVER FLOW FORECASTING THROUGH CONCEPTUAL MODELS PART I - A DISCUSSION OF PRINCIPLES. *Journal of Hydrology*, 10, 282–290.
- Taddese, G. (2001). Land Degradation: A Challenge to Ethiopia. *Environmental Management*, 27, 815–824. <http://dx.doi.org/10.1007/s002670010190>
- Taylor, K. E. (2001). *in a single diagram*. 106, 7183–7192.
- Tegegne, G., & Melesse, A. M. (2020). Multimodel Ensemble Projection of Hydro-climatic Extremes for Climate Change Impact Assessment on Water Resources. *Water Resources Management*, 34(9), 3019–3035. <https://doi.org/10.1007/s11269-020-02601-9>
- Temesgen Gashaw, Amare Bantider, and H. G. (2014). Gully Rehabilitation & Stabilisation Fact Sheet. *Adigrat University*, 4(9).
- Tesemma, Z.K., Mohamed, Y.A., Steenhuis, T. S. (2010). Trends in rainfall and runoff in the Blue Nile Basin: 1964–2003. *Hydrol. Process.*, 24.
- Tesfa Yimer. (2015). *Hydrological modeling of a Maybar watershed using Arc SWAT, Awash Basin, Amhara Region*. May.
- Theron, S. N., Weepener, H. L., Le Roux, J. J., & Engelbrecht, C. J. (2021). Modelling potential climate change impacts on sediment yield in the Tsitsa river catchment, South Africa. *Water SA*, 47(1), 67–75. <https://doi.org/10.17159/wsa/2021.v47.i1.9446>
- Tsegaye, B. (2019). Effect of Land Use and Land Cover Changes on Soil Erosion in Ethiopia. *International Journal of Agricultural Science and Food Technology*, 5, 26–34.
- Tsitsagia, M., Berdzenishvilib, A., & M. Gugeshashvilia. (2018). Spatial and temporal variations of rainfall-runoff erosivity (R) factor in Kakheti, Georgia. *Annals of Agrarian Science*, 16, 226–235.
- Wallace, C. W., Flanagan, D. C., Engel, B. A., & C. W. Wallace, D. C. Flanagan, B. A. E. (2017). QUANTIFYING THE EFFECTS OF FUTURE CLIMATE CONDITIONS

- ON RUNOFF, SEDIMENT, AND CHEMICAL LOSSES AT DIFFERENT WATERSHED SIZES. *American Society of Agricultural and Biological Engineers*, 60(3), 915–929. <https://doi.org/10.13031/trans.12094>
- Wang, G., Mang, S., Cai, H., Liu, S., Zhang, Z., Wang, L., & Innes, J. L. (2016). Integrated watershed management: evolution, development and emerging trends. *Journal of Forestry Research*, 27(5), 967–994. <https://doi.org/10.1007/s11676-016-0293-3>
- White, K. L., & Chaubey, I. (2005). Sensitivity analysis, calibration, and validations for a multisite and multivariable SWAT model. *Journal of the American Water Resources Association*, 41(5), 1077–1089. <https://doi.org/10.1111/j.1752-1688.2005.tb03786.x>
- Williams, J. R. (1975). Sediment yield prediction with universal equation using runoff energy factor. *Proceedings of the SedimentYield Workshop*.
- Woldemariam, A., Getachew, T., & Chanie, T. (2023). Long-term trends of river flow , sediment yield and crop productivity of Andit tid watershed , central highland of Ethiopia. *All Earth*, 35(1), 3–15. <https://doi.org/10.1080/27669645.2022.2154461>
- Xiong, Y., Ta, Z., Gan, M., Yang, M., Chen, X., Yu, R., Disse, M., & Yu, Y. (2021). Evaluation of CMIP5 climate models using historical surface air temperatures in central asia. *Atmosphere*, 12(3), 1–11. <https://doi.org/10.3390/atmos12030308>
- Yates, D., & Strzepe, K. (1994). Potential Evapotranspiration Methods and their Impact on the Assessment of River Basin Runoff Under Climate Change. In *International Institute for Applied Systems Analysis*.
- Yesuf, H. M., Assen, M., Alamirew, T., Melesse, A. M., & Yesuf, H.M., Assen, M., Alamirew, T., Melesse, A. M. (2015). Modeling of sediment yield in Maybar gauged watershed using SWAT, northeast Ethiopia. *Catena*, 127, 191–205. <https://doi.org/10.1016/j.catena.2014.12.032>
- Yu, Y.-S., Zou, S., Whittemore, D. (1993). Non-parametric trend analysis of water quality data of rivers in Kansas. *J. Hydrol.*, 150, 61–80.
- Yuan, L., & and Kenneth J. Forshay. (2020). Using SWAT to evaluate streamflow and lake sediment loading in the xinjiang river basin with limited data. *Water (Switzerland)*, 12(1), 1–20. <https://doi.org/10.3390/w12010039>
- Zhang, D., Lin, Q., Chen, X., & Chai, T. (2019). Improved curve number estimation in SWAT by reflecting the effect of rainfall intensity on runoff generation. *Water (Switzerland)*, 11(163). <https://doi.org/10.3390/w11010163>
- Zhang, S., Li, Z., Lin, X., & Zhang, C. (2019). Assessment of Climate Change and Associated Vegetation Cover Change on Watershed-Scale Runoff and Sediment Yield. *Water*, 11(07), 1373.
- Zhang, X., Srinivasan, R., & Hao, F. (2007). Predicting hydrologic response to climate change in the Luohe River basin using the SWAT model. *Transactions of the ASABE*, 50(3), 901–910. <https://doi.org/10.13031/2013.23154>